ARTICLE

Chromite compositional variability and associated PGE enrichments in chromitites from the Gomati and Nea Roda ophiolite, Chalkidiki, Northern Greece

Micol Bussolesi[1] · Giovanni Grieco[2] · Federica Zaccarini[3] · Alessandro Cavallo[1] · Evangelos Tzamos[4] · Niccolò Storni[2]

Abstract

The Gomati and Nea Roda ophiolites are located into the Serbo-Macedonian massif of the Chalkidiki peninsula (Northern Greece). The present work focuses on the variability of platinum-group elements (PGEs), geochemistry, spinel mineral chemistry, and platinum-group minerals (PGMs) — base metal minerals (BMMs) assemblage in chromitites of three Gomati localities (St. George, Tripes, and Limonadika) and Nea Roda. The studied chromitites show variable textures and are heavily altered. Primary silicates are almost completely replaced by chlorite, and chromite rims are altered into ferrian chromite. The variability of spinel mineral chemistry in terms of Cr# [Cr/(Cr + Al)] and Mg# [Mg/(Mg + Fe^{2+})], and the PGE contents, argues for a genesis in a supra-subduction setting (SSZ), at different stratigraphic positions in the ophiolite section. Chromitites from Tripes have the lowest Cr# (0.5–0.6) and the highest PGE contents (3516 ppb), similar to some chromitites formed in small magma chambers in the cumulate sections above the Moho. The high PGE contents of Tripes chromitites are due to an IPGEs-enriched melt derived from critical melting of mantle peridotites. Limonadika and St. George show the highest Cr# (0.77–0.96 and 0.74–0.87, respectively) and variable PGE contents (175 ppb and 383 ppb on average respectively), compatible with a genesis from boninitic magmas in the mantle section. Nea Roda chromitites have intermediate to high Cr# (0.66–0.75) and low PGE contents (135 ppb on average) and show similarities to other intermediate chromitites formed from evolving magma sources at subduction initiation. BMMs detected in both ophiolites are primary (pentlandite) and secondary (mainly millerite and heazlewoodite) sulfides. All the detected PGMs are primary, crystallized from the melt, and entrapped into chromite, and they are mainly laurites. In the studied chromitites, the absence of alloys indicates that the circulating fluids during chloritization were at high fS$_2$ and fO$_2$, and did not remobilize the PGEs. The same fluids are probably responsible for the low-T crystallization of an uncommon suite of arsenides and antimonides at St. George.

Keywords Platinum group elements · Supra-Moho · Chromitite · Greece · Ophiolites

✉ Micol Bussolesi
micol.bussolesi@gmail.com

1 Department of Earth and Environmental Sciences - DISAT, University of Milan-Bicocca, P.zza della Scienza 1-4, 20126 Milan, Italy

2 Department of Earth Sciences, University of Milan, via S. Botticelli 23, 20133 Milan, Italy

3 Department of Applied Geological Sciences and Geophysics, University of Leoben, 8700 Leoben, Austria

4 Ecoresources PC, Giannitson and Santarosa Str., 15-17, 54627 Thessaloniki, Greece

Introduction

Ophiolite-hosted chromitite bodies can be found scattered within the mantle section and across the Moho transition zone. Several works report the coexistence of chromitites with heterogeneous Cr# in the same ophiolite complex (Uysal et al. 2016; Qiu et al. 2018; Liu et al. 2019). Chromitites are thus classified as high-Al (Cr# < 0.50), intermediate (0.50 < Cr# < 0.70), and high Cr (Cr# > 0.70) (Uysal et al. 2016), although some authors distinguish only between high-Cr (Cr# > 0.60) and high-Al (Cr# < 0.60) chromitites (e.g., Zhou et al. 1998; Xiong et al. 2017). According to classic genetic models, Cr-poor chromitites form at mid-ocean ridges (Uysal et al. 2009; Arai and Miura 2015), back-arc
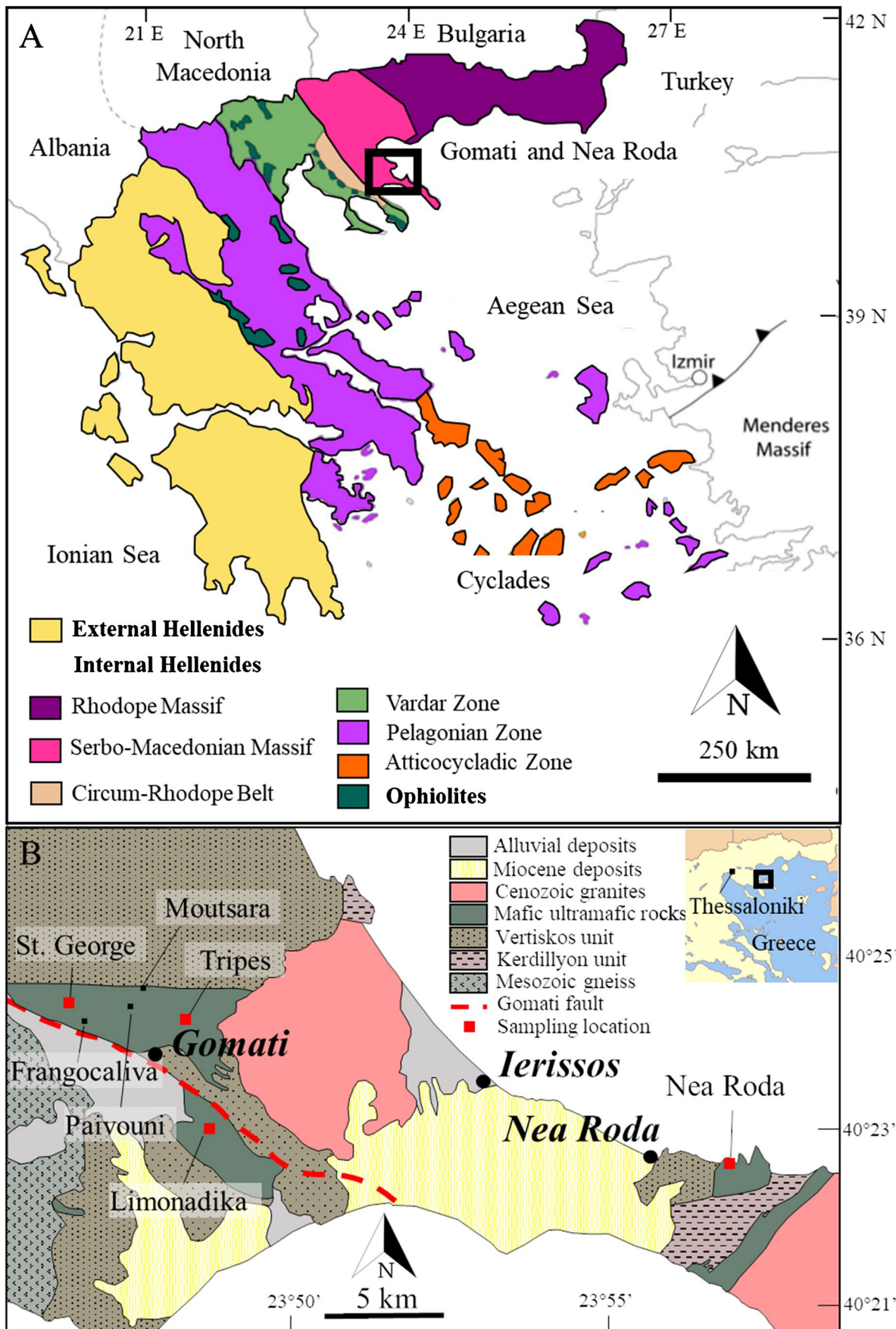
◄**Fig. 1 A** Major structural elements of the Aegean Sea region, modified after Cornelius (2008) and Zachariadis (2007). **B** Modified excerpt of the 1:50,000 scale geological map of the Ierissos sheet, with location of old chromitite mines

settings (González-Jiménez et al. 2011), or in the supra-Moho cumulate sequence of ophiolite complexes, where they occur as concordant layers alternated to pyroxenite and peridotite cumulates (Stowe 1994; Garuti et al. 2012). High-Cr chromitites, on the other hand, are interpreted to be generated in the depleted mantle section of ophiolites in supra-subduction zone (SSZ) settings (Zhou and Robinson 1997).

In more recent years, Cr# variability in the same ophiolite complex has been interpreted as a progressive evolution of parental melt from MORB-like to boninitic at subduction initiation (Uysal et al. 2016, 2018; Qiu et al. 2018; Chen et al. 2019; Liu et al. 2019; Bussolesi et al. 2022).

Ophiolite chromitites are variably enriched in PGEs, from tens to several hundreds of ppb (Economou et al. 1986; Prichard and Tarkian 1988; Andrews and Brenan 2002; Gervilla et al. 2005; González-Jiménez et al. 2014a; Zaccarini et al. 2016). Podiform chromitites are usually enriched in IPGEs (Os, Ru, Ir) with respect to PPGEs (Pt, Pd, Rh) (Ahmed and Arai 2002; Grieco et al. 2020), but occasionally, also Pt–Pd-enriched chromitites can be found (Prichard et al. 2008).

PGEs in the primitive mantle are hosted within a monosulfide solid solution (MSS) (Lorand and Alard 2001). During partial melting, IPGEs and Rh tend to remain in the residual mantle, while Pt and Pd behave as incompatible elements and fractionate into the melt (Ballhaus et al. 2006). For this reason, high-Al chromitites formed in a mid-ocean ridge or back-arc setting are usually PGE-poor (Prichard et al. 2008). At higher degrees of partial melting, all PGEs are dissolved into the melt and are more likely to produce PGE-rich high-Cr chromitites with a high IPGE/PPGE ratio. High-Al, supra-Moho chromitites show highly variable PGE contents, from the PGE-poor chromitites of the Oman ophiolite (Ahmed and Arai 2002) to the PGE-rich chromitites of the Nurali massif (Zaccarini et al. 2004; Grieco et al. 2007).

PGEs and base metals, hosted within sulfides, are often remobilized during alteration events. The most common alteration event, affecting ophiolite ultramafic rocks, is serpentinization. During such events, PGMs and BMMs in contact with the fluids undergo desulfurization, and PGEs and other metals are remobilized (Grieco et al. 2020).

The Gomati and Nea Roda ophiolites (Northern Greece) host numerous chromitite bodies with heterogeneous spinel mineral chemistry and variable PGE enrichments. In this paper, we aim to contribute to the study of Gomati and Nea Roda high-Cr and intermediate chromitites and their associated PGE contents, by means of chromite major and trace

element composition. Moreover, we reconstruct the remobilization of PGEs and base metals (BMs) within chromitites altered by circulation of high fS_2 and high fO_2 chloritizing fluids.

Geological setting

Gomati and Nea Roda are two ophiolite bodies located in the Chalkidiki peninsula, Northern Greece, ~ 80 km SE of the city of Thessaloniki.

The Chalkidiki peninsula is a geologically complex region, which comprises several geotectonic zones, belonging to the Hellenides belt, tectonically emplaced during the Mesozoic to Cenozoic evolution of subduction and collision. The Hellenides, part of the Alpine-Himalayan orogenic belt, can be divided into two tectonic units: External and Internal Hellenides. The Internal Hellenides are furtherly divided in tectonic zones. The main ones are from west to east: Pelagonian zone (PZ), Atticocycladic zone (AZ), Vardar zone, Circum-Rhodope belt (CRB), Serbo-Macedonian massif (SMM), and Rhodope massif (RM), all roughly oriented NNW-SSE (Anders et al. 2006). Gomati and Nea Roda ophiolites are comprised into the SMM, which is separated from the PZ to the west by a suture, the Vardar zone, hosting several Jurassic ophiolite bodies. To the east, the SMM borders the Rhodope massif (Fig. 1A).

The Serbo-Macedonian massif (SMM) and the Rhodope massif (RM), extending through Serbia, North Macedonia, Greece, and Bulgaria, consist of amphibolite-facies metamorphic rocks forming the basement of the Alpine orogenic belt (Dixon and Dimitriadis 1984; Ricou et al. 1998; Himmerikus et al. 2009; Bonev and Dilek 2010; Bonev et al. 2013, 2018; Šoster et al. 2020). A later Cenozoic extension is recorded by Late Cretaceous to Miocene granitoid intrusions outcropping in both massifs (Ricou et al. 1998; Bonev et al. 2012). Mafic–ultramafic bodies are present in nearly all the crystalline basement of SMM and RM, overlying Middle to Late Paleozoic-Triassic platform carbonate rocks (Papanikolaou 2013).

The SMM is divided into two units, the Kerdyllion unit and the Vertiskos unit, separated by a SW-dipping thrust (Kockel et al. 1971; Kockel 1977). The Kerdyllion unit, cropping out in the eastern part, is composed of migmatized gneisses and schists intruded by Triassic to Cenozoic granitoid rocks (Himmerikus et al. 2009). The Vertiskos unit, cropping out in the central part of the SMM, consists of an alternation of gneisses and schists, hosting mafic–ultramafic bodies, known as the Therma-Volvi-Gomati (TGV) complex (Kockel 1977; Dixon and Dimitriadis 1984). The TGV complex has been interpreted as a dismembered ophiolite formed in the Early Triassic before the opening of the Vardar Ocean (Dixon and Dimitriadis 1984).

The Gomati ultramafic complex, hosted in the Vertiskos unit, is cut by the Gomati fault, which separates the ophiolite bodies of northern Gomati from those of southern Gomati (Fig. 1B).

Serpentinized peridotite is the predominant lithology of Gomati (Christodoulou 1980). Serpentinized and fresh dunite were recognized at Frangocaliva, and serpentinized harzburgite with bastite was found at Moutsara, whereas at Tripes and Paivouni dunite-pyroxenite associations, as well as amphibolite layers alternated to serpentinite, are reported (Christodoulou 1980). Chromite is an accessory phase always present within these lithologies. Small chromite deposits, exploited in the past, can be found in different localities in the complex. The contact between chromitites and their host lithologies (variably altered dunites and/or clinopyroxenites), when visible, is always sharp (Christodoulou 1980).

The wild vegetation covering the territory makes it difficult to properly recognize field relations and to perform field work. Chromite mines are not visible anymore, and chromite ore was found in stocks at the coordinates indicating the entrance to St. George, Tripes, and Limonadika closed mines (Kockel et al. 1978; Christodoulou 1980). At St. George, numerous blocks of chromite ore and associated rocks up to 60 cm thick have been found in the bed of a dry river. These chromitites (up to 60% chromite modal content) are in contact with chloritized clinopyroxenites. At a distance of approximately 100-m north of the locality, serpentinites crop out through the vegetation. Tripes was the most difficult area to access, due to the vegetation and the steep inclines. A sample of massive chromitite was found in a small heap of rocks close to the coordinates indicated by the geological map, and it probably represents the chromitite stock of Tripes mine. Serpentinites crop out at a distance of 50 m from the stock. Limonadika is the only chromite mine in the southern Gomati ophiolite. Massive chromitites and serpentinites have been found in a stock. Amphibolites and magnesites are also present in the area.

The Nea Roda ophiolite is an ultramafic body located 15 km east of the Gomati village, thrust onto the basement of the Vertiskos unit. It consists of harzburgites hosting dunite dykes, with serpentinization degrees ranging from 20 to 100% (Michailidis et al. 1995). Small chromitite bodies with disseminated to nodular textures are hosted within dunite dykes (Michailidis et al. 1995; Bussolesi et al. 2022). Close to these outcropping chromite occurrences, massive chromitite blocks form a small stock of ore on the Nea Roda beach.

Analytical methods

Mineral chemistry of chromites and silicates from samples TRI10A, TRI10B, LIM-1, LIM-3, and NRO-9 was determined through a JEOL 8200 electron microprobe equipped

with a wavelength dispersive system (SEM-WDS) at the Earth Sciences Department of the University of Milan. Samples GOM2A, GOM2B, GOM2C, GR54A, GR54C, GR54D, and GR55 were analyzed through a JEOL 8200 electron microprobe at the Eugen F. Stumpfl Laboratory at the University of Leoben, Austria.

PGE analyses have been performed on 6 chromitites from St. George, Tripes, and Limonadika and on three Nea Roda chromitites. Samples up to 25 g in size were fire assayed using a nickel sulfide (NiS) fire assay procedure and later analyzed through instrumental neutron activation analysis (INAA) at Actlabs laboratory in Canada. Detection limits for each element are 2 ppb (Os), 0.1 ppb (Ir), 5 ppb (Ru), 0.2 ppb (Rh), 5 ppb (Pt), 2 ppb (Pd), and 0.5 ppb (Au).

Trace elements in chromites were detected using a quadrupole-inductively coupled plasma-mass spectrometry and ThermoFisher Scientific iCAP RQ coupled with an excimer laser Teledyne CETAC Technologies Analyte Excite 193 nm equipped with a HelEx 2 volume sample cell at LASA laboratory (University of Milan). Raw data were elaborated using the software Glitter. Operation conditions of the instrumentation are reported in Appendix 1.

Petrography

St. George

Chromitites at St. George are associated with chloritized clinopyroxenite and rare wehrlite. The contact between chromitite and clinopyroxenite is sharp (Fig. 2A). Chromitites form massive (> 80% chromite modal content) and disseminated (60–70% chromite modal content) bands of variable thickness, ranging between 5 mm and 30 cm. Chromite crystals have euhedral to subhedral shape and contain abundant chlorite inclusions, generally oriented along the crystal planes of the host chromite, and filling pores generated by ferrian chromite alteration. Primary silicates are mostly replaced by Cr-chlorite (Fig. 2B), and the only preserved relics are clinopyroxene crystals. Ferrian chromitization is widespread and mainly occurs along rims and cracks. The cores of large crystals are unaltered (Fig. 2C), while smaller ones are completely altered.

The associated clinopyroxenite and minor wherlite are also heavily altered. Clinopyroxene is the only primary silicate preserved within clinopyroxenite, while primary olivine is also preserved within wehrlite. Chlorite is the main secondary silicate, replacing clinopyroxene and olivine (Fig. 2D). The groundmass consists of fine-grained chlorite and serpentine aggregates. Accessory Cr-spinel is mainly subhedral and completely altered into ferrian chromite.

PGMs are fairly abundant within St. George. They are all euhedral laurite crystals found as inclusions within
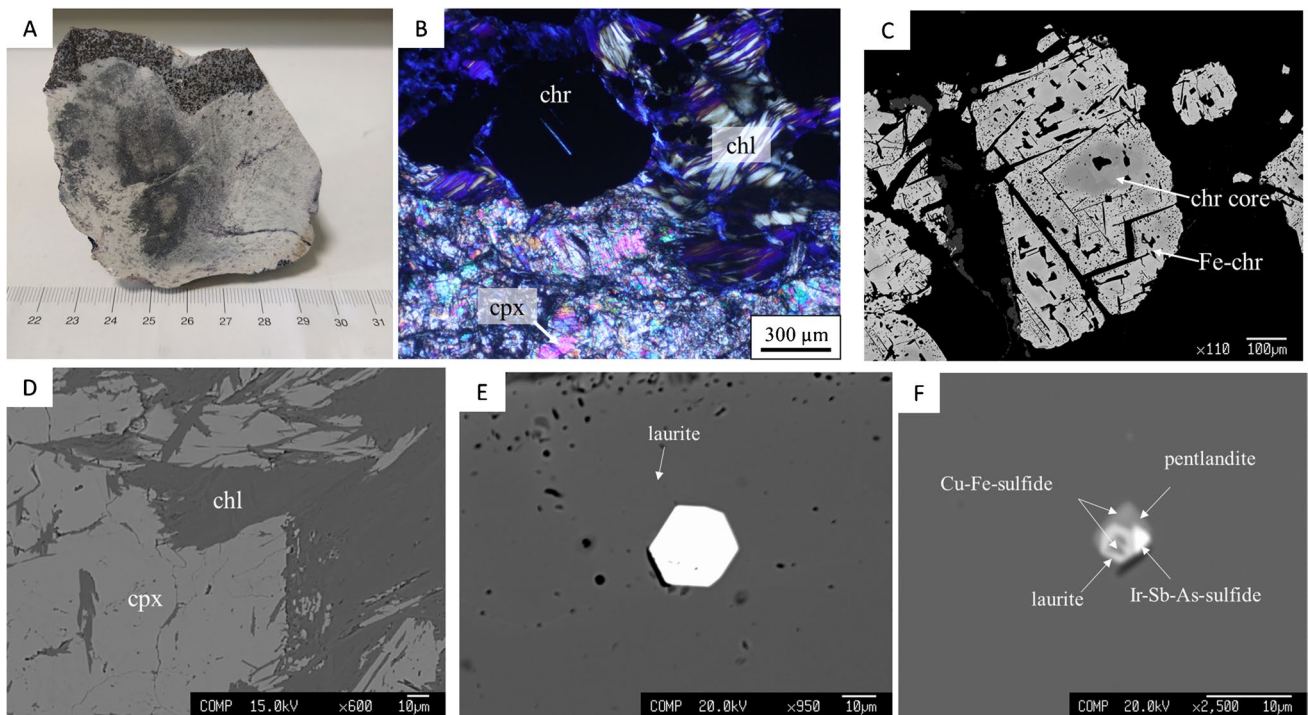
Fig. 2 Hand sample (**A**), XPL (**B**, **C**), and BSE (**D** to **F**) images of chromitites and associated host rocks from St. George, Gomati. **A** Hand sample showing the contact between chromitite (black) and clinopyroxenite (light gray). **B** Chloritized chromitite in contact with clinopyroxenite host rock. **C** Ferrian chromite altered grain with a fresh chromite core. **D** Partial replacement of clinopyroxene by chlorite crystals. **E** Euhedral laurite crystal within chromite core. **F** Polyphasic grain of laurite, pentlandite, Ir-Sb-As-S phase, and Cu-Fe sulfide

unaltered chromite (Fig. 2E), either as a single phase or associated to other sulfides, generally Ni-Cu sulfides, antimonides, or arsenides (Fig. 2F). Their size is variable but generally lower than 20 µm. They rarely display zonations.

BMMs at St. George are abundant both in chromitites and their associated clinopyroxenites. The assemblage comprises Ni–Fe sulfides, arsenides, and antimonides. Rare pentlandite ($(Fe, Ni)_9S_8$) is the only BMM included within unaltered chromite (Fig. 3A). Other sulfides, arsenides, and antimonides are distributed in the silicate matrix or included in ferrian chromite. Heazlewoodite (Ni_3S_2) is the most abundant BMM (Fig. 3B), followed by millerite (NiS) (Fig. 3C), arsenides (maucherite $Ni_{11}As_8$, orcelite $Ni_{5-x}As_2$, $\times \sim 0.23$ and Ni_3As), and rare Cu-Fe sulfides. St. George clinopyroxenites show a peculiar arsenide-antimonide assemblage, described by Bussolesi et al. (2020).

The only known arsenide phases detected within clinopyroxenites are orcelite and a mineral with a formula approaching dienerite (Ni_3As) (Fig. 3D). Of the antimonides, the only identified mineral is breithauptite (NiSb) (Fig. 3E), while the other Sb phases are undetermined minerals (Bussolesi et al. 2020). Moreover, crystals of

parkerite ($Ni_3(Bi, Pb)_2S_2$, Fig. 3F) and shandite ($Pb_2Ni_3S_2$) have been detected.

Tripes

The chromitite sample at Tripes has a massive texture, with > 90% chromite modal content. Chromite crystals have euhedral to subhedral shape. They are fractured, and the rims are partially altered into ferrian chromite (Fig. 4A). Primary silicates have been completely replaced by Cr-chlorite, and relict clinopyroxene was found only very locally. Serpentinites associated with chromitites show clinopyroxene and olivine relicts, with size ranging between 100 and 300 µm, scattered in a fine serpentinitic and chloritic groundmass. Accessory spinel forms subhedral crystals with a maximum size of 100 µm, partially or completely altered into ferrian chromite.

PGMs are abundant within the Tripes chromitites. They consist mostly of euhedral grains enclosed in unaltered chromite, with size ranging between 1 and 15 µm. Only in one case the PGM grain has an anhedral shape. Most PGMs belong to the laurite-erlichmanite series (Ru, Os) S_2 occurring as monomineralic grains or associated with other sulfides (Fig. 4B). A total of five undetermined
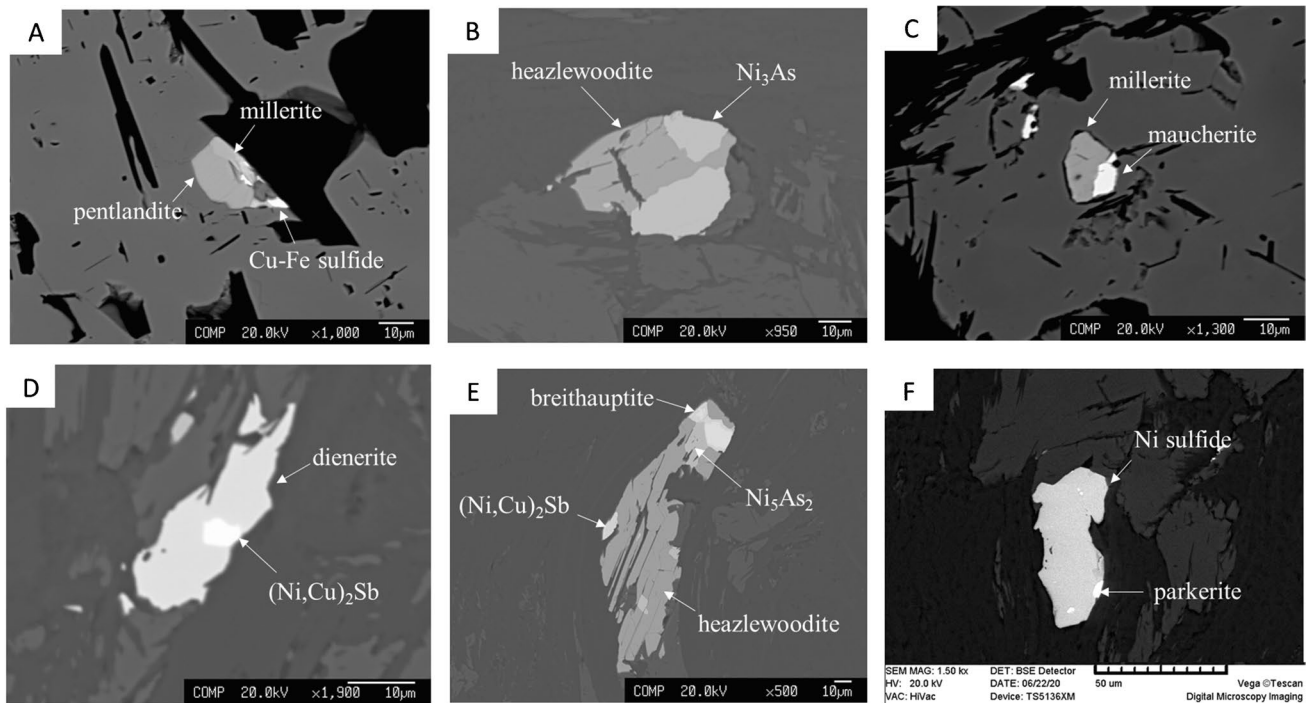
Fig. 3 BSE images of base metal minerals at St. George. **A** Polyphasic grain of pentlandite, millerite, and a Cu-Fe-sulfide. **B** Heazlewoodite and Ni arsenide at St. George (modified after Bussolesi et al. (2020). **C** Polyphasic grain of millerite and maucherite. **D** Mineral approaching dienerite stoichiometry associated with an undetermined Ni-Cu antimonide. **E** Undetermined Ni-Cu antimonide and Ni arsenide in association with breithauptite and heazlewoodite. **F** Parkerite crystal associated with a Ni sulfide

Fig. 4 BSE images (**A** to **D**) and X-ray elemental maps (**E**) of Tripes chromitites. **A** Massive chromite with ferrian chromite rims and interstitial chlorite. **B** Laurite associated with pentlandite. **C** Ru-Os-Ir-Ni–Fe sulfide with millerite, pentlandite, and an undetermined Fe-sulfide. **D** Ir-Rh-Pt-Ni–Fe-Cu sulfide associated with a Ni–sulfide and a Fe-sulfide. **E** X-ray elemental maps of grain (**D**)

PGMs were also detected in the samples. They are one Ru-Os-Ir-Ni–Fe sulfide (Fig. 4C) and four Ir-Rh-Ni–Fe-Cu sulfides with similar compositions (Fig. 4D and E).

The BMM assemblage is scarce and comprises Ni–Fe sulfides (pentlandite and millerite), rare pyrite, and nickeline (NiAs).

Limonadika

Chromitites from Limonadika are massive, with 70–80% chromite modal content. They are characterized by coarse chromite grains in a chloritic silicate matrix. Chromite crystals have euhedral to subhedral shape; they are fractured, and the rims are altered into ferrian chromite. Primary silicates have been completely replaced by Cr-chlorite (Fig. 5A). PGMs were not detected in this area. The BMM assemblage is scarce and consists mainly of nickeline and millerite filling pores produced by chromite alteration (Fig. 5B).

Nea Roda

Chromitites sampled at Nea Roda were collected from an ore stock on the beach, close to a harzburgite-dunite outcrop. They are massive chromitites, with a chromite modal content > 80%. Chromite crystals are mostly subhedral and anhedral, and the crystal size is highly variable, from ten to several hundred microns. Chromites are fractured, and chromite rims are altered into ferrian chromite (Fig. 6A). PGMs are rare, and only one laurite

crystal was found (Fig. 6B). BMMs are not as abundant as in St. George and are mostly Ni–Fe sulfides included within chromite.

Mineral chemistry

Chromite mineral chemistry

Unaltered chromite average compositions (ESM Table 1) are based on core analyses (Appendix 2). The composition of the spinels is rather heterogeneous among the different localities.

At St. George, chromitite shows high Cr#, comprised between 0.74 and 0.87, and Mg# between 0.22 and 0.55. The composition of chromites shows significant variations in MgO (4.18 and 9.85 wt%), FeO (14.03 and 26.80 wt%), Fe_2O_3 (0.00–6.72 wt%), Cr_2O_3 (51.13 and 65.54 wt%), and Al_2O_3 (6.08 and 12.44 wt%).

At Tripes, chromitite has lower Cr#, ranging between 0.57 and 0.61 and Mg# between 0.37 and 0.56. Spinel composition shows MgO (8.37 and 12.27 wt%), FeO (16.87 and 25.29 wt%), Fe_2O_3 (3.15 and 7.60 wt%), Cr_2O_3 (41.58 and 45.66 wt%), and Al_2O_3 (18.99 and 19.73 wt%).

At Limonadika, chromitite is high Cr, with Cr# (0.77–0.96) and Mg# (0.36–0.51). The composition of chromite is more similar to St. George, with MgO (7.19 and 10.71 wt%), FeO (17.96 and 23.04 wt%), Fe_2O_3 (0.95 and 3.81wt%), Cr_2O_3 (57.69 and 68.38 wt%), and Al_2O_3 (2.04 and 11.73 wt%).

At Nea Roda, chromitite shows a composition intermediate between Tripes and St. George, with Cr# between
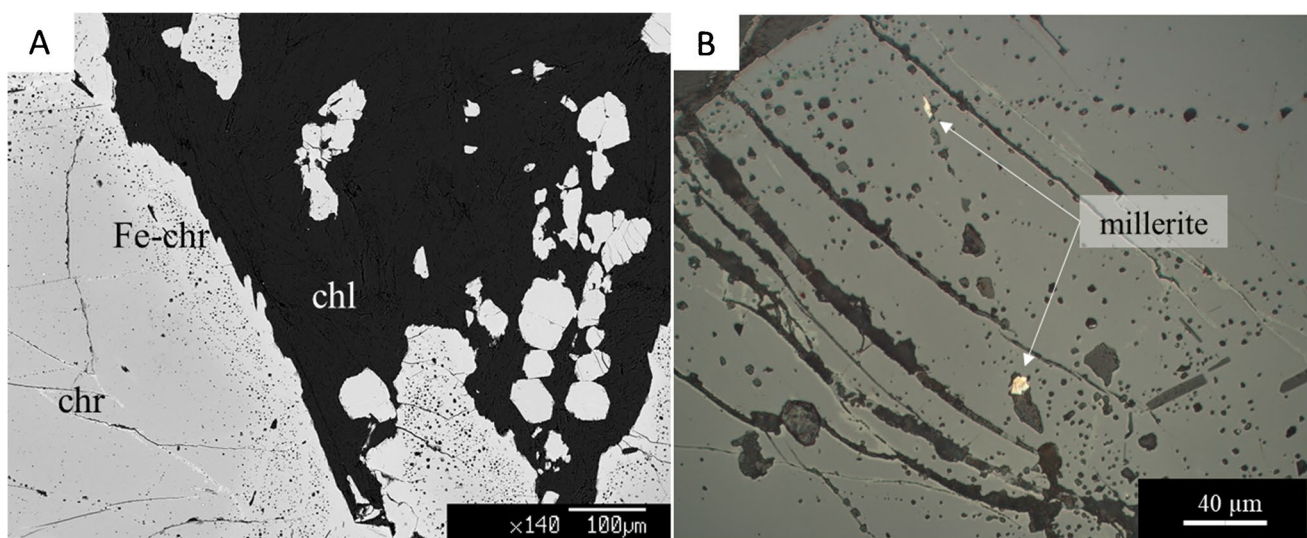

Fig. 5 **A** BSE image of Limonadika chromitites showing the chloritic groundmass and ferrian chromite rims. **B** PPL image in reflected light of millerite crystals filling chromite pores
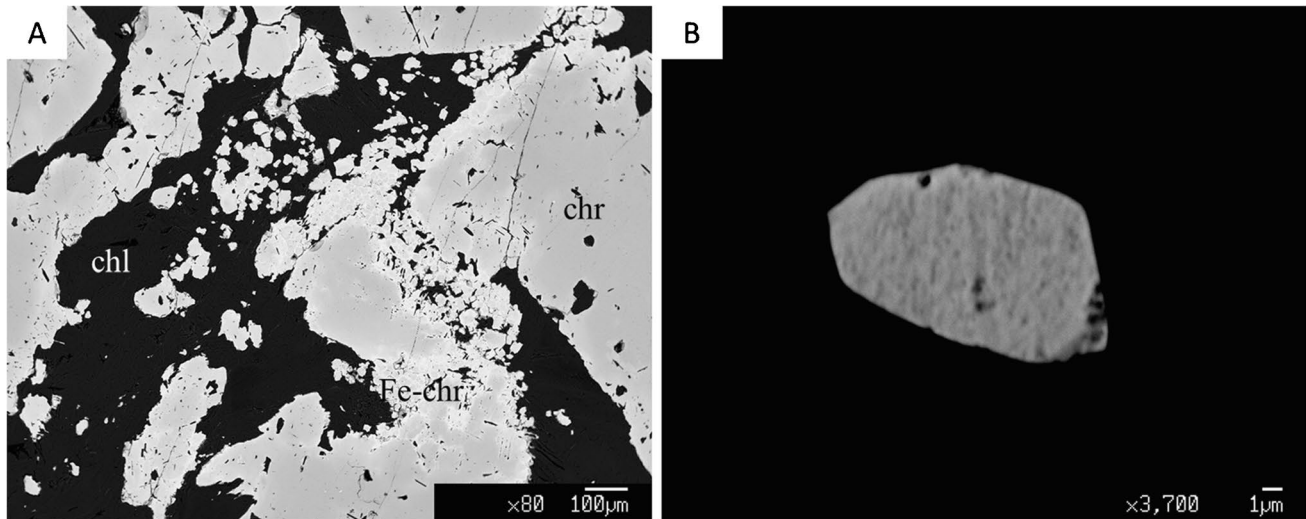
Fig. 6 BSE images of **A** texture of Nea Roda chromitites. **B** Laurite crystal enclosed within chromite at Nea Roda

0.66 and 0.75 and Mg# between 0.56 and 0.63. Spinel composition shows MgO (12.37 and 14.22 wt%), FeO (14.72 and 16.26 wt%), Fe_2O_3 (1.06 and 1.23 wt%), Cr_2O_3 (52.68 and 57.97 wt%), and Al_2O_3 (18.86 and 21.18 wt%).

Spinels from different chromitites sampled in the Gomati ultramafic complex show Mg# values between 0.20 and 0.60 and very different Cr# values among them (Fig. 7A). Limonadika chromites have the highest Cr#,
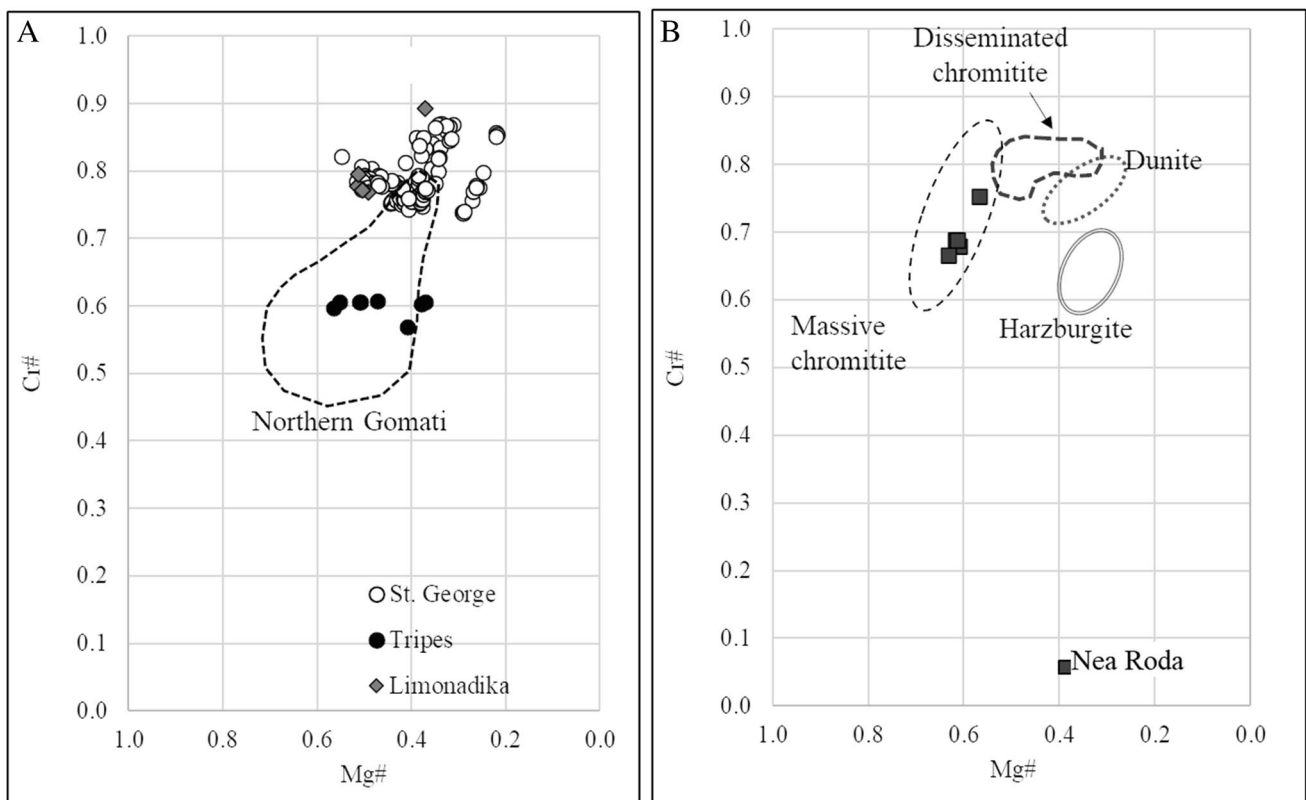

Fig. 7 Mg# vs Cr# values of Gomati (**A**) and Nea Roda (**B**). Compositional field of northern Gomati is from Christodoulou (1980); massive chromitite, disseminated chromitite, dunite, and harzburgite compositional fields are from Michailidis et al. (1995)

ranging between 0.77 and 0.90. St. George chromites have slightly lower Cr# (0.74 to 0.87), partially overlapping the Limonadika field. Tripes chromites show the most different Cr# values, ranging between 0.57 and 0.61. Chromite compositions in the three localities partially fit with data from Christodoulou (1980) on spinels from both massive and disseminated chromitites of northern Gomati. Nea Roda spinels display Cr# values comprised between 0.67 and 0.75, fitting into the Nea Roda massive chromitite compositional field defined by Michailidis et al. (1995) (Fig. 7B).

According to Uysal et al. (2016) classification, St. George and Limonadika chromitites can be defined "high-Cr," Tripes chromitites "intermediate," and Nea Roda chromitites varying from "intermediate" to "high Cr." However, the Mg# of St. George, Limonadika, Tripes, and Nea Roda is generally lower than other intermediate chromitites (e.g., Antalya, Pozanti-Karsanti, and Guleman intermediate ophiolite chromitites) (Fig. 8A) and can be compared to Nurali level 1, level 2, CHR-II, and Kraubath chromitites, formed in the cumulate sequence above the Moho (Fig. 8B). Based on Al_2O_3 and TiO_2 vs Cr_2O_3
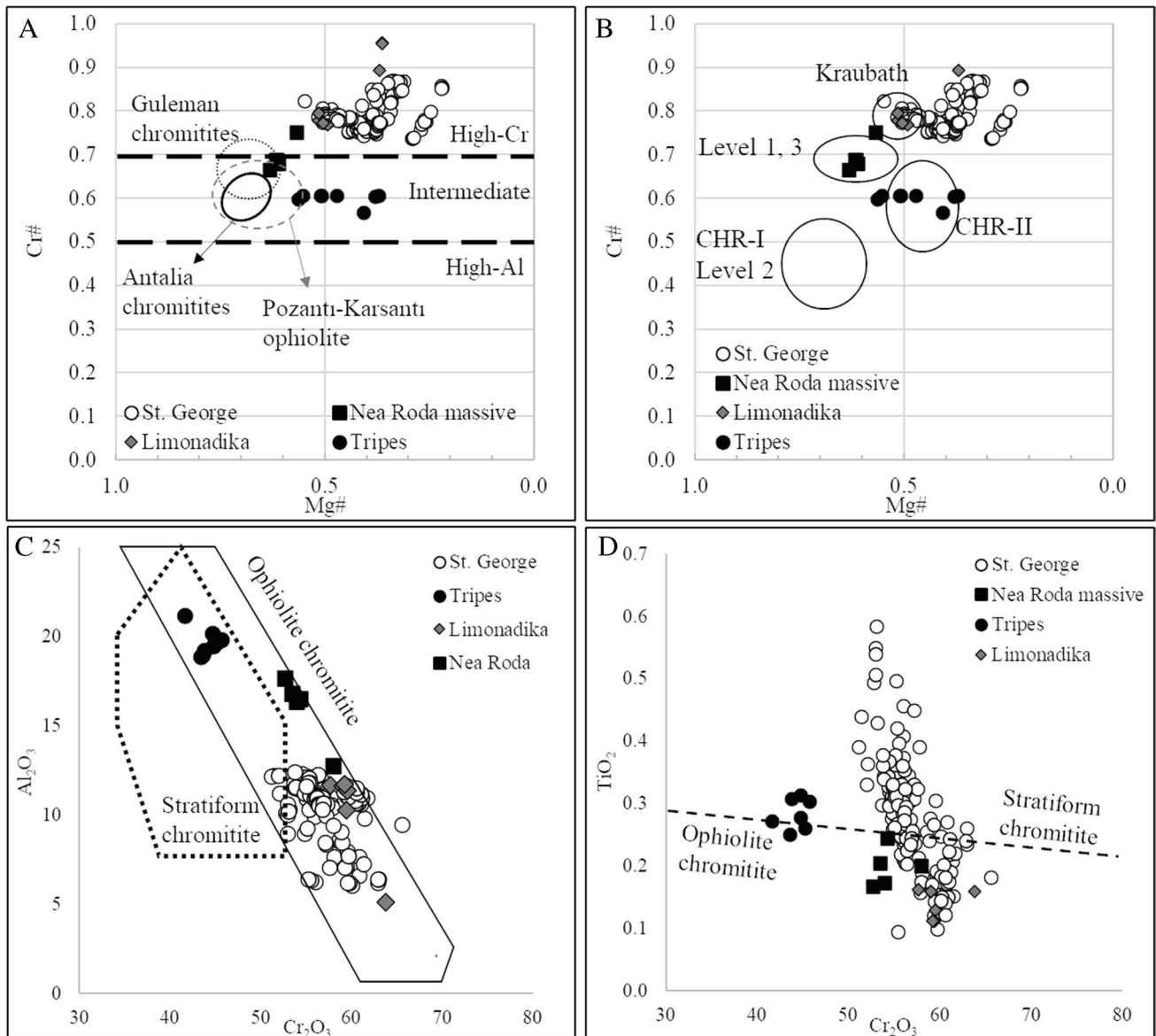

Fig. 8 Chemical composition of chromite from Gomati and Nea Roda chromitites and comparison between stratiform and podiform chromitites and with supra-Moho chromitites. **A** and **B** Mg# vs Cr#. **C** Cr_2O_3 vs Al_2O_3. **D** Cr_2O_3 vs TiO_2. Compositional fields for Antalya, Pozanti-Karsanti, and Guleman intermediate chromitites are from Uysal et al. (2016, 2018) and Liu et al. (2019). Podiform and stratiform compositional fields are from Arai et al. (2004), compositional fields of Nurali CHR-I and CHR-II are from Zaccarini et al. (2004), of Nurali level 1, level 2, and level 3 are from Grieco et al. (2007), and of Kraubath are from Malitch et al. (2003)

contents, St. George and Limonadika high-Cr chromitites show affinity with typical ophiolite chromitites, Tripes intermediate chromitites are more similar to stratiform ones, and Nea Roda chromitites have a composition intermediate between Tripes and Gomati but plot mostly in the ophiolite chromitite compositional field (Fig. 8C and D).

Trace element contents (Appendix 2, ESM Table 2) of unaltered chromite cores show low amounts of Sc (0.48–5.26 ppm), Ga (9.1–54.3 ppm), Ge (0.46–2.48 ppm), and Co (86–516 ppm), comparable to other ophiolitic chromitites (Zhou et al. 2014). V and Mn contents are similar at Tripes (822 and 2819 ppm on average), St George (788 and 1828 ppm on average), and Nea Roda (919 and 1854 ppm on average) but higher at Limonadika (1162 and 4085 ppm

on average). Zn content is highly variable among the localities, with average of 1367 ppm at Tripes, 738 ppm at St. George, 988 ppm at Limonadika, and 532 ppm at Nea Roda. Ni average content is higher at Tripes (1121 ppm) than at St. George (501 ppm), Limonadika (596 ppm), and Nea Roda (645 ppm).

In order to compare the data, trace elements have been normalized to the chromite of the East Pacific Rise MORB (Pagé and Barnes 2009) and compared to high-Cr chromitites and high-Al chromitites of podiform and stratiform deposits. The patterns show similarities (Ti and Zn positive anomalies) but also significant variations. Chromitites from Tripes (Fig. 9A) are enriched in Ti, Zn, Co, and Mn and depleted in Sc. Chromites from St. George massive
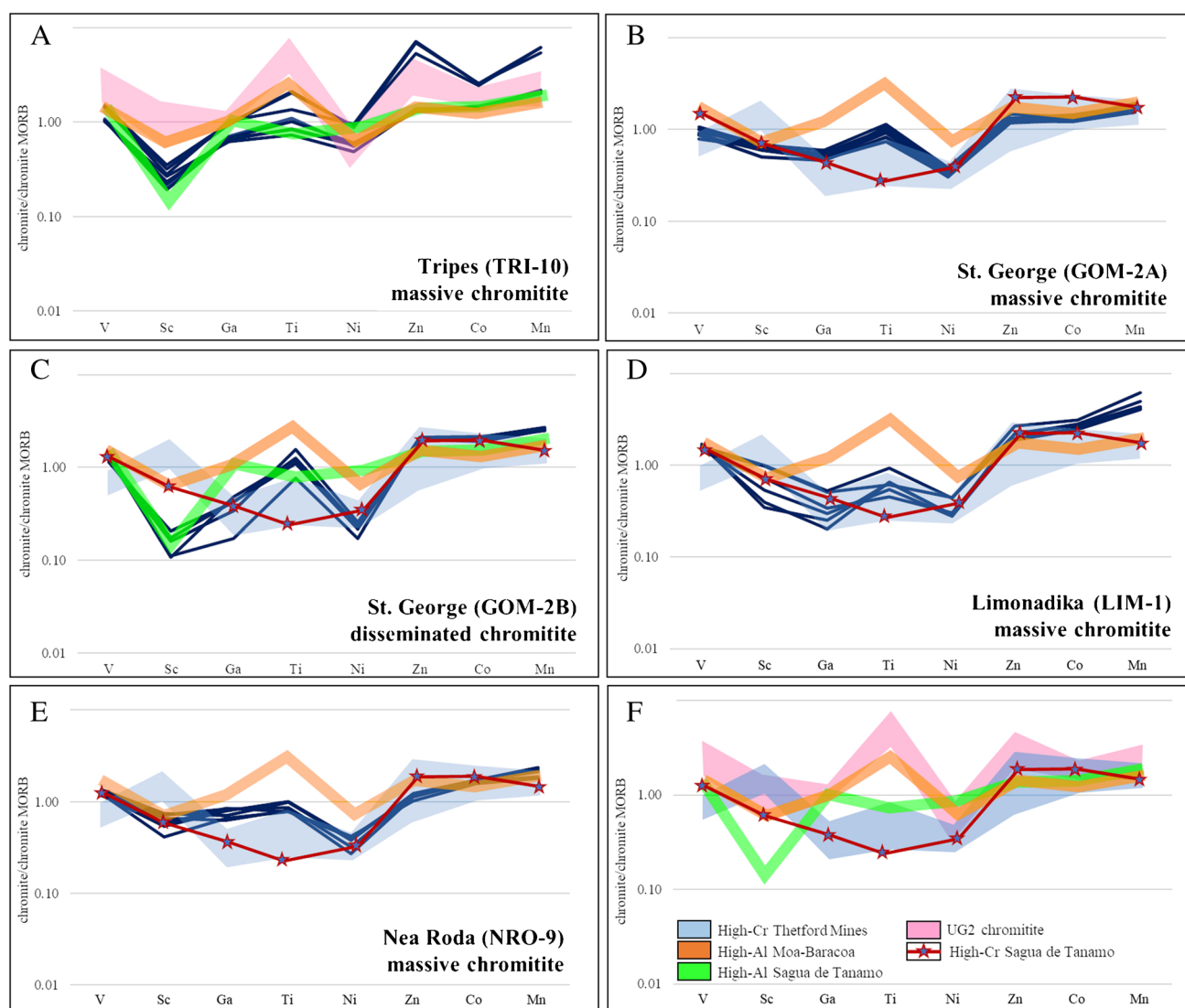

Fig. 9 Spider diagrams showing the composition of minor and trace elements of chromite cores (blue lines), normalized to MORB chromites (Pagé and Barnes 2009). Data sources for comparison are Thetford Mines chromites (Pagé and Barnes 2009), Moa-Baracoa chromites (Zhou et al. 2014), Sagua de Tanamo chromites (González-Jiménez et al. 2014b), and UG-2 chromites (Langa et al. 2021)

chromitites (Fig. 9B) are slightly enriched in Ti, Zn, Co, and Mn. They do not show a Sc-negative anomaly but only a slight Ti-positive anomaly. Chromites from disseminated chromitite at St. George (Fig. 9C) have a pronounced Sc-negative anomaly and a slight Ti-positive anomaly. Massive chromitites from Limonadika (Fig. 9D) and Nea Roda (Fig. 9E) show patterns similar to St. George massive chromitites.

Silicate mineral chemistry

Primary silicates within chromitites are almost completely replaced by chlorite. The only relicts found are clinopyroxene crystals, rich in Ca (20.22–26.08wt% CaO) and Mg (17.50–23.30wt% MgO) and Al-free. The composition of the clinopyroxenes within chromitites and clinopyroxenites is the same in all the studied samples, and based on their stoichiometric formula $(Ca_{0.80-1.02}Na_{0.00-0.02})(Mg_{0.97-1.28}Fe_{0.00-0.02})(Si_{1.86-2.04}Al_{0.00-0.04})O_6$, they can be classified as diopsides and augites (Appendix 3). In one sample from St. George, Mg-rich olivine crystals were found in the clinopyroxenites associated with the chromitites. Within the clinopyroxenites of St. George, chlorite and serpentine crystals partially replace primary silicates (clinopyroxene and minor olivine). Chlorite composition within chromitites and clinopyroxenites is homogeneous. The analyzed chlorites, according to Hey (1954) calibration, are all clinochlore with stoichiometric formula $Mg_{9.8}Fe_{0.2}Cr_{0.6}Al_{1.4}Si_{6.11}Al_{1.9}O_{20}(OH)_{16}$ and penninite with stoichiometric formula $Mg_{9.8}Fe_{0.2}Cr_{0.7}Al_{1.1}Si_{6.4}Al_{1.6}O_{20}(OH)_{16}$, with some grains of talc-chlorite and a single sheridanite, found at Tripes. However, due to the presence of abundant Cr_2O_3 (up to 5

wt%), which was found in all of the analyzed chlorites, the term chromian clinochlore to define Gomati chlorites is more appropriate. Serpentine was found exclusively within chromitite host rocks, where it forms part of the silicate matrix.

Platinum-group minerals and base metal minerals mineral chemistry

PGMs were detected at St. George, Tripes, and Nea Roda (ESM Table 3). At St. George, the totality of PGMs belongs to the laurite-erlichmanite series. Few grains display a zonation, with the rim enriched in Os with respect to the core. The crystals have variable Ru-Os contents, and the mineral formulas range from $(Ru_{0.6}Os_{0.2}7Ir_{0.07}Rh_{0.02}Pd_{0.02}S_{1.99})$ to $(Ru_{0.77}Os_{0.15}Ir_{0.03}S_{1.99})$ (Fig. 10A). The highest number of PGMs was detected at Tripes, where minerals of the laurite-erlichmanite series are the most abundant. The crystals do not show zonations, and the mineral formulas range from erlichmanite $(Os_{0.66}Ru_{0.26}S_{2.02})$ to laurite $(Ru_{0.80}Os_{0.11}Ir_{0.03}S_{1.99})$ (Fig. 10A). Tripes chromitites also contain two undetermined PGE sulfides. One of them is a Ni-Ir-Fe-Cu-Rh sulfide with mineral formula $Ni_{0.38}Ir_{0.26}Fe_{0.18}Cu_{0.12}Rh_{0.03}S$, while the other is a Ru-Ir-Fe sulfide with mineral formula $Ru_{0.50}Ir_{0.2}Fe_{0.15}Os_{0.04}Cu_{0.04}S_2$ (Fig. 10B). At Nea Roda, only one homogeneous laurite grain with mineral formula $Ru_{0.74}Os_{0.16}Ir_{0.07}S_{2.01}$ was detected (Fig. 10A).

Base metal minerals detected in Gomati and Nea Roda are sulfides (ESM Table 4), arsenides (ESM Table 5), and antimonides (Appendix 4).

St. George has a quite rich BMM assemblage, comprising heazlewoodite (Ni_3S_2), millerite (NiS), pentlandite $(Fe,Ni)_9S_8$, chalcocite (Cu_2S), an undetermined
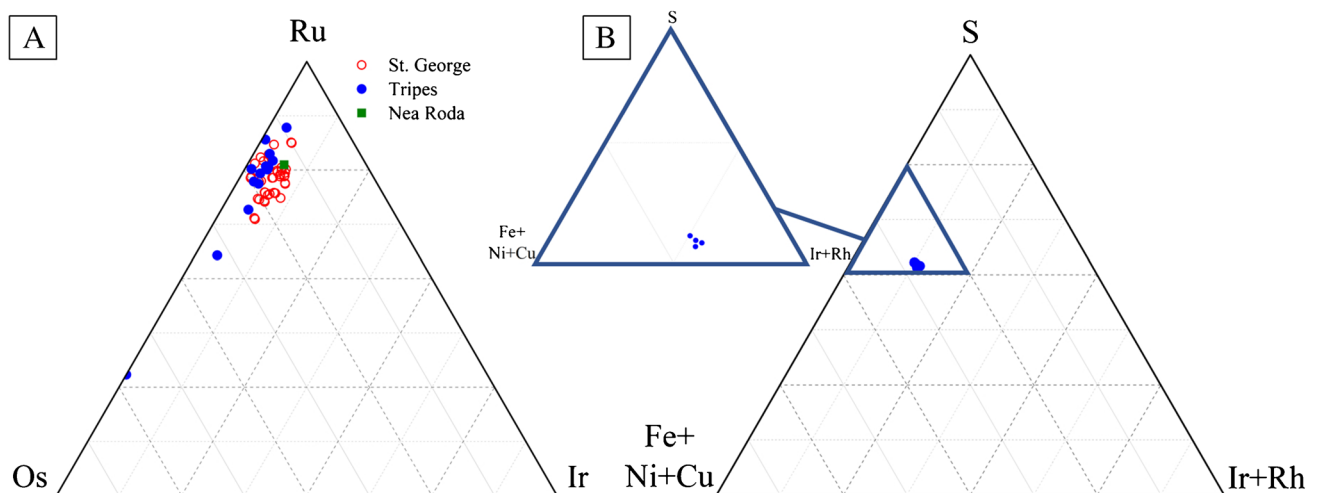

Fig. 10 Ternary compositional diagrams (at%) of **A** PGM of the laurite-erlichmanite series at Gomati and Nea Roda and **B** undetermined Ni-Ir-Fe-Cu sulfides at Tripes
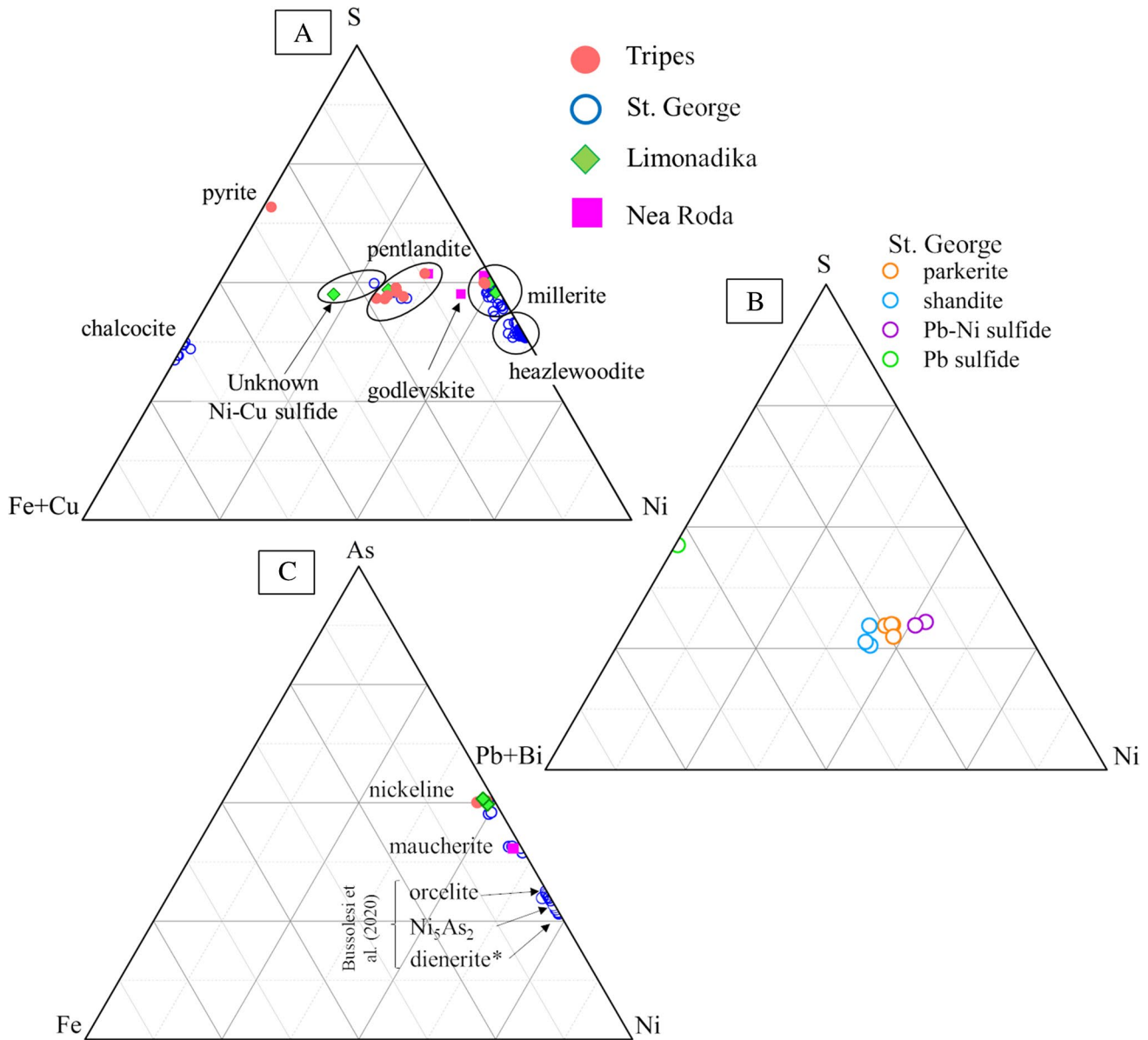
Fig. 11 Ternary compositional diagrams (at%) of **A** Ni–Fe-Cu sulfides, **B** Ni-Pb-Bi sulfides, and **C** Ni–Fe arsenides within Gomati and Nea Roda

Fe-Cu-Ni sulfide (Fig. 11A), shandite ($Pb_2Ni_3S_2$), parkerite ($Ni_3(Pb,Bi)_2S_2$), Pb-Ni sulfides (Fig. 11B), maucherite ($Ni_{11}As_8$), nickeline (NiAs), dienerite (Ni_3As), Ni_5As_2, orcelite ($Ni_{5-x}As_2$ ($x = 0.23$) (Fig. 11C), and rare antimonides. Of the sulfides, heazlewoodite shows PGE enrichments (Ir up to 0.23 wt%, Pt up to 0.64 wt%), and pentlandite is enriched in Pt up to 0.48 wt%. Maucherite is the most abundant Ni-arsenide, followed by nickeline and orcelite. Two analyzed minerals are undetermined species. Their recalculated mineral formulas are Ni_3As and Ni_5As_2 (Bussolesi et al. 2020). Four antimonide species have been detected at St. George (Bussolesi et al. 2020). The minerals are

abundant within the serpentinized clinopyroxenites associated with massive chromitites, and rare within massive chromitites, where they are found within the silicate gangue.

The BMM assemblage at Tripes comprises mainly pentlandites and some millerite and nickeline grains (Fig. 11A). Pentlandite is enriched in some PGEs (up to 0.57 wt% Ir, up to 1.10 wt% Rh, up to 0.72 wt% Pt). Millerite is enriched in Ir (up to 0.66 wt%) and Pt (up to 0.62 wt%).

At Limonadika, the BMM assemblage comprises millerite, pentlandite, an undetermined Fe–Ni-Cu sulfide, pentlandite, and nickeline (Fig. 11A). Millerites show a slight

enrichment in Pt, up to 0.12 wt%, and the only pentlandite grain detected is enriched in Pt up to 0.19 wt%.

At Nea Roda, the BMM assemblage comprises millerite, godlevskite, and maucherite (Fig. 11A). Millerite has residual Fe contents up to 1 wt%. Godlevskites show enrichments in PGE, such as Ir (up to 0.40 wt%), Os (up to 0.16 wt%), and Pt (up to 0.68 wt%). The only maucherite detected shows enrichments in Ir (0.14 wt%) and Rh (= 0.10 wt%).

Bulk-rock contents of platinum-group elements

The total PGE content (ESM Table 6) ranges between 125 and 3516 ppb, with a general high IPGE/PPGE ratio. Chromitites from St. George have ΣPGEs ranging between 331.9 and 418.8 ppb, and IPGE/PPGE comprised between 15.30 and 18.73. Tripes chromitite shows an anomalous high PGE content (3516 ppb) and a relatively low IPGE/PPGE of 7.90. Limonadika is the locality in Gomati with the lowest amount of ΣPGEs (175.2 ppb) and with IPGE/PPGE of 8.63. Chromitites from Nea Roda are the poorest in PGEs, with ΣPGE ranging between 125.6 and 146.7 ppb, and with IPGE/PPGE comprised between 13.47 and 18.56.

Discussion

Gomati and Nea Roda tectonic setting and magmatic evolution

Evidences from chromite mineral chemistry

The coexistence of high-Cr, intermediate, and high-Al chromitites in the same ophiolite complex has been explained in the literature by an evolving parental magma from MORB-like to boninitic-like at subduction initiation (Uysal et al. 2016, 2018; Chen et al. 2019; Liu et al. 2019).

High Al_2O_3 and relatively high TiO_2 contents in spinel are also typical of ophiolite chromitites that occur within or above the Moho transition zone (MTZ) (Zaccarini et al. 2004; Grieco et al. 2007), generally defined as the zone comprised between the mantle and the crustal sections of ophiolites (Malitch et al. 2003). Chromitites from Tripes and partially St. George, Limonadika, and Nea Roda are comparable in composition to the Nurali MTZ chromitites from southern Urals (Zaccarini et al. 2004) (Fig. 8B). The Nurali massif is an ophiolite body comprising a lherzolitic mantle section and a supra-Moho ultramafic cumulate sequence. The cumulate sequence hosts small chromitite bodies at different stratigraphic levels. These bodies differ in texture and composition, from high-Cr, PPGE-rich chromitites in the lower level (level 1, CHR-II), intermediate, and PGE-rich chromitites at an intermediate level (level 2, CHR-I), to high-Cr PGE-poor chromitites at the uppermost level (level 3)

(Grieco et al. 2007). The genesis of Nurali supra-Moho chromitites is more similar to stratiform chromitite deposits than to podiform ones. It involves the crystallization of spinels within a magma chamber, triggered by the mixing between an intruding primitive melt and a chemically evolved resident melt (Grieco et al. 2007; Garuti et al. 2012), akin to the formation of stratiform chromitites in the Bushveld complex (Naldrett et al., 2008 and references therein).

Chromitites from Tripes have spinel Cr#, Mg#, and PGE contents comparable to Nurali CHRII supra-Moho chromitites. Their Cr# is also similar to intermediate chromitites, formed from MORB-like melts at subduction initiation (e.g., Guleman, Antalia, and Pozanti-Karsanti ophiolite chromitites) (Fig. 8A), but their Mg# is lower, and the PGE content is too high to infer a genesis from MORB-like melts.

Nea Roda massive chromitite spinels have a composition similar to those from Nurali level 1 and level 3 chromitites. The former are high-Cr chromitites generated above the Moho in the first stages of partial melting of primitive mantle, and the latter are generated from the further melting of a mantle source depleted in PGEs by earlier melting events (Grieco et al. 2007). Nonetheless, the intermediate composition of Nea Roda chromitites is also in agreement with a genesis in the mantle, from an arc-type melt that precipitated high-Cr chromites leaving behind a low-Cr# and PGE-poor residual melt (Uysal et al. 2016).

St. George and Limonadika chromitites are high Cr and have an affinity with typical chromitites generated from boninitic magmas in the mantle. However, St. George chromitites also display some features in common with chromitites generated closely above the MTZ, such as the association with clinopyroxenite and rarely wehrlite (Garuti et al. 2012).

Trace elements in chromites have been studied in few localities, and only those of the Moa Baracoa and Sagua de Tanamo districts, Cuba, are supra-Moho chromitites, stratigraphically positioned above the MTZ (Zhou et al. 2014).

The Sc-negative and Ti-positive anomalies of Tripes trace elements patterns (Fig. 9A) are comparable to the high-Al podiform chromitites of the Moa-Baracoa district in Cuba, formed in a back-arc environment (González-Jiménez et al. 2011) close to the mantle-crust transition zone (Proenza et al. 1999a, b; Zhou et al., 2001), but Zn, Co, and Mn enrichments are comparable only to those of the UG2 level in the Bushveld layered intrusion, implying a genesis from fractional crystallization inside a magma chamber. Moreover, Ti-positive anomalies in chromitite trace element patterns are regarded as clues of crystallization close to the mantle-crust transition zone (Proenza et al. 1999b; Rollinson 2008), pointing towards a supra-Moho genesis for Tripes chromitites.

The trace element patterns of St. George massive and disseminated chromitites (Fig. 9B and C), Limonadika

(Fig. 9D), and Nea Roda (Fig. 9E) are comparable to other high-Cr chromitites, like those of the Thetford Mines in Canada (Pagé and Barnes 2009) or the Sagua de Tanamo district of Cuba (Zhou et al. 2014), indicating a boninitic parental magma, generated by relatively high degrees of partial melting within the mantle.

Evidences from PGM and BMM assemblage

PGMs within Tripes, St. George, Limonadika, and Nea Roda chromitites were found only as primary inclusions within chromites. Due to the inclusion relationship and their euhedral shape, the PGMs are interpreted as magmatic in origin and formed at the same time or slightly prior to chromite crystallization. The assemblage is quite homogeneous, made up mainly by minerals of the laurite-erlichmanite series (Fig. 10A). Experimental studies (Brenan and Andrews 2001; Bockrath et al. 2004) show that Os-free laurite can crystallize in equilibrium with Os-Ir alloys at 1200–1300 °C, at $logfS_2$ ranging from -2 to -1.3, and that Os solubility in laurite increases with decreasing temperature and/or increasing fS_2. González-Jiménez et al. (2009) suggested that different Os contents within laurites could reflect their crystallization in a dynamic regime, with increasing fS_2 conditions, which can occur during cooling.

Laurites and other IPGE-rich phases are the most common PGMs within ophiolite chromitites (González-Jiménez et al. 2014a; Grieco et al. 2020), while PPGE-rich minerals are usually associated with stratiform chromitites (Naldrett et al. 2008). Supra-Moho chromitites show high variability, from IPGE-rich to PPGE-rich chromitites. PGE-rich supra-Moho chromitites from the Nurali massif are characterized by an abundance of laurite crystals included in chromite (level 2) and by the presence of Pd–Pt PGMs interstitial to chromite in level 1 (Zaccarini et al. 2004; Grieco et al. 2007). Kraubath banded chromitites, formed in the transition zone at the base of the cumulate sequence above the Moho (Malitch et al. 2003), also show PPGE-enriched minerals.

While St. George, Limonadika, and Nea Roda PGM assemblage is common to the majority of ophiolite chromitites, the abundance of PGMs within Tripes, and the variability of the PGM species, is more similar to Nurali level 2 chromitites.

The undetermined Ni-Ir-Fe-Cu sulfides found in Tripes have stoichiometry approaching Me/S 1:1 (Fig. 10B). Minerals with a similar composition were detected within the Ojen lherzolite massif in Spain (Torres-Ruiz et al. 1996), within mantle tectonites of the Tiebaghi massif of New Caledonia (Legendre and Augé 1986) and in the Finero complex (Garuti et al. 1990). These minerals have been classified as PGE-rich sulfides. They could be a PGE-rich variety of pyrrhotite, especially considering that Ir and Rh have a preferential solubility within this mineral (Cabri and Laflamme

1981). However, the possibility that they are a new mineralogical species cannot be excluded.

Pentlandite was solely found as euhedral crystals within unaltered chromite, and it was therefore assessed as the only primary BMM. Ni–Fe-Cu BMMs within ophiolite chromitites are generated upon the separation of an immiscible sulfide melt during the early stages of crystallization of basic melts forming pyrrhotite, chalcopyrite, and later pentlandite (Kullerud 1969). Pentlandite appears when pyrrhotite breaks up below 610 °C to form a pentlandite-pyrrhotite association that, below 550 °C, can be altered into a pentlandite-heazlewoodite association (Kullerud 1969).

Primary BMMs and PGMs are more abundant within Tripes with respect to the other localities. This could be due to the high chromite modal content, which favors the preservation of primary sulfides within unaltered chromite grains.

Evidences from PGE contents

PGEs in the primitive mantle are hosted within a monosulfide solid solution (MSS) (Lorand and Alard 2001). The PGE content of a melt is therefore dependent on the degree of partial melting of the primitive mantle and on the dissolution of the MMS within the melt. Chromitites enriched in PGEs crystallize in equilibrium with melts formed in a critical melting interval of 20–25%, identified by Prichard et al. (2008). Lower degrees of melting would produce PGE-poor chromitites, or the extraction of PPGEs, which are less refractory than IPGEs (e.g., basaltic melts formed beneath spreading centers) (Economou-Eliopoulos 1996; Ahmed and Arai 2002; Gervilla et al. 2005; González-Jiménez et al. 2011). On the contrary, higher degrees of melting would dilute the PGE contents, especially Pt and Pd, which fractionate into the melt (Brenan and Andrews 2001). Arc-related melts forming above subduction slabs are usually generated by degrees of partial melting $> 20\%$ and are therefore rich in PGEs. This is the case for ophiolitic chromitites, with high IPGE/PPGE ratios (Economou-Eliopoulos, 1996; Grieco et al., 2020 and references therein), while chromitites in the Moho transition zone show highly variable IPGE/PPGE ratios (Malitch et al. 2003; Zaccarini et al. 2004; Grieco et al. 2007).

The PGE contents of Tripes, St. George, Limonadika, and Nea Roda chromitites are in agreement with the PGM suite detected within the samples, both in terms of IPGE/PPGE ratios and PGE relative abundances.

The PGE content of Tripes chromitites can be compared only to Nurali level 2, enriched in IPGEs relative to PPGEs, deriving from the remelting of a residual mantle depleted in Pt and Pd (Zhou et al. 1998; Zaccarini et al. 2004; Grieco et al. 2007) (Fig. 12A).

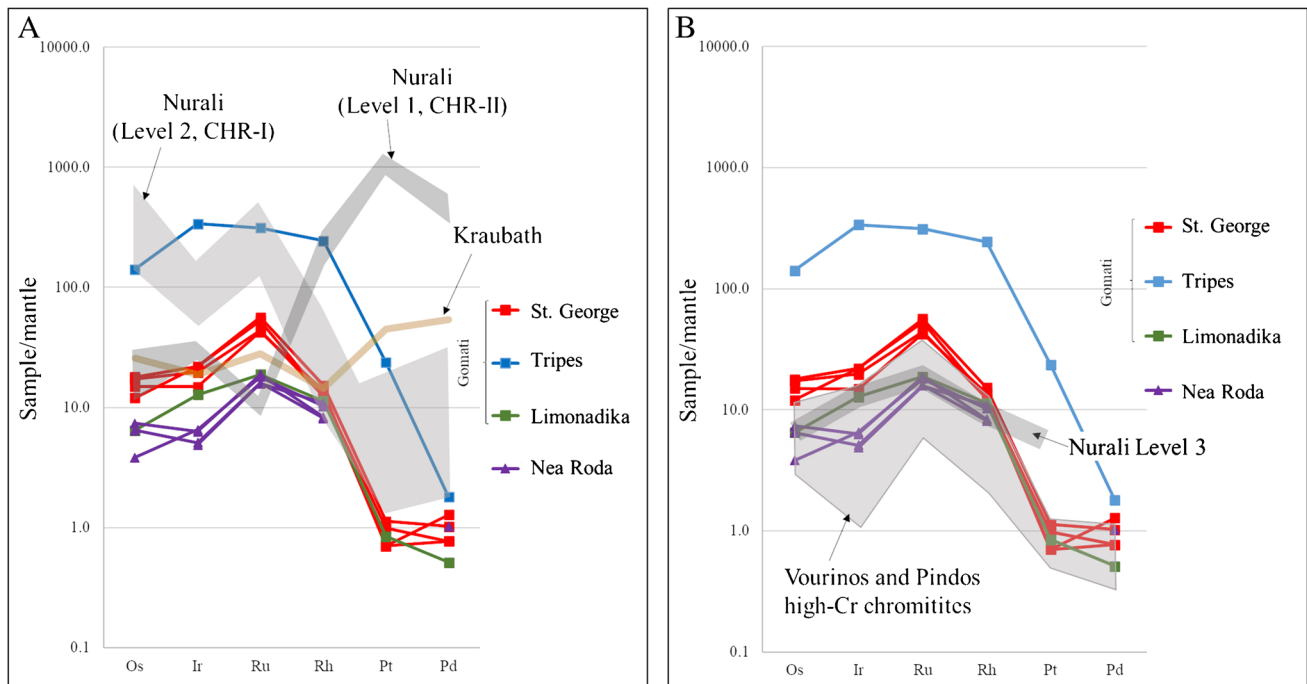Chromitites from Nea Roda show PGE contents quite similar to Nurali level 3, the uppermost level of the

Fig. 12 Mantle-normalized (McDonough and Sun 1995) patterns of Gomati and Nea Roda chromitites compared to **A** supra-Moho chromitites from Nurali (Zaccarini et al. 2004; Grieco et al. 2007) and Kraubath (Malitch et al. 2003) and **B** Vourinos and Pindos high-Cr ophiolite chromitites (Economou-Eliopoulos 1996)

supra-Moho cumulate sequence, generated from the further melting of an already PGE-depleted mantle source, and therefore PGE-poor (Grieco et al. 2007). However, Nea Roda PGE contents are also comparable to typical high-Cr chromitites, and they cannot help to define with certainty the stratigraphical position of this complex within the ophiolite sequence (Fig. 12B).

St. George and Limonadika PGE contents are also comparable to typical high-Cr chromitites, enriched in IPGEs with respect to PPGEs, for example, those of the Vourinos and Pindos ophiolites, located in the External Hellenides and showing the same PGE-normalized patterns as Limonadika and St. George (Fig. 12B).

Overview of tectonic setting and magmatic evolution of Gomati and Nea Roda chromitites

The variability in spinel mineral chemistry, ranging from intermediate (Tripes and Nea Roda) to high Cr (St. George and Limonadika), could suggest an evolution of the parental melt from MORB to boninitic in a SSZ setting. However, the high PGE total content of Tripes intermediate chromitites is not compatible with a genesis from a MORB-like melt, which would produce PGE-poor chromitites. On the other hand, PGE contents, PGM variability, and spinel mineral chemistry are comparable to some supra-Moho chromitites (e.g., Nurali ophiolite), strongly supporting an origin within

or above the Moho transition zone. Tripes was likely formed by melts derived from the partial melting of a Pd–Pt-poor mantle source, where the MSS was completely melted, releasing all its PGE contents. The abundance of PGMs in 6, moreover, suggests that it formed within the critical melting interval, probably in a supra-subduction zone setting and not in a back-arc setting.

Nea Roda chromitites are similar in composition and PGE contents both to Nurali level 3 chromitites, formed above the Moho, and to intermediate chromitites formed in the mantle from an arc-type melt that had previously precipitated high-Cr chromites leaving behind a low-Cr# and PGE-poor residual melt (Uysal et al. 2016), and therefore, its origin remains uncertain.

St. George and Limonadika high-Cr chromitites show PGE-normalized patterns, PGM assemblage, and chromite mineral chemistry comparable to typical high-Cr mantle chromitites, and they were likely generated from boninitic magmas in a supra-subduction setting. Nevertheless, it should be mentioned that the association of St. George chromitites with clinopyrixenites is a feature in common with some chromitites formed in the cumulate sequence above the Moho (Garuti et al. 2012).

Low-T post-magmatic evolution

Evidences from chromite and silicate mineral chemistry

Massive chromitites from Gomati and Nea Roda ultramafic complexes, and their associated host rocks (clinopyroxenite and rare wehrlite, associated to St. George chromitites, and dunite associated to Tripes, Limonadika and Nea Roda) show widespread alteration, and the dunites are completely altered into serpentinites. Rare clinopyroxene relicts are the only primary silicates found within chromitites, scattered in a chlorite matrix, and within the clinopyroxenites. Clinopyroxenes are partially replaced by chlorite (Fig. 2B, D). Chloritization of massive chromitites is a well-known process which was described in several mafic ultramafic massifs. Many studies report the formation of Cr-chlorite and ferrian chromite within chromitites during low-T hydrothermal alteration (Merlini et al. 2009; Kapsiotis 2015; Colás et al. 2019). Colás et al. (2017) and Gervilla et al. (2012) describe the reaction between primary chromite and olivine in the presence of SiO_2-rich fluids, producing clinochlore and Fe-rich chromite, under water-saturated and reducing conditions.

González-Jiménez et al. (2009) and Kimball (1990) propose the formation of chlorite and ferrian chromite through the reaction of chromite with MgO- and SiO_2-rich fluids. González-Jiménez et al. (2009) suggest that temperatures up to 300 °C could favor the serpentinization of olivine and pyroxenes and create the MgO- SiO_2-rich environment necessary for the formation of chlorite and ferrian chromite.

Several studies report replacement of clinopyroxene by chlorite, a process that takes place at low T and P (Good et al. 1997; Helgadóttir et al. 2015; Centrella et al. 2018). This suggests that chlorite and ferrian chromite described in the studied massive chromitites from the Gomati and Nea Roda ultramafic complexes could have been formed at the expense of primary clinopyroxene and chromite. An alternative hypothesis to explain the formation of chlorite and ferrian chromite could be the transformation of clinopyroxene into serpentine and subsequent reaction of serpentine with chromite to form chlorite and ferrian chromite, with complete obliteration of serpentine during the reaction.

Evidences from PGM and BMM assemblage

Secondary PGMs within ophiolite chromitites are usually found within the silicate matrix and can be recognized by corroded rims or complete replacement by alloys (Grieco et al. 2020). No secondary PGMs were found in the studied chromitites from the two ultramafic complexes, as all the PGMs are included in unaltered chromite grains and have euhedral shape.

Secondary BMMs form subhedral to anhedral crystals within the silicate matrix or in the altered ferrian chromite rims. Tripes, due to its high chromite modal content, is poor in secondary BMMs. St. George chromitites are dominated by heazlewoodite, millerite, and chalcocite. Ni-Pb-Bi sulfides in the form of shandite, parkerite, and an undetermined Pb-Ni sulfide (Fig. 11B) were also found at St. George, as well as an uncommon suite of arsenides and antimonides. Limonadika and Nea Roda are the localities with fewer BMMs, mostly heazlewoodite, millerite, and godlevskite. No alloy was detected in either of the two ultramafic complexes (Fig. 11A). This suggests that fO_2 and fS_2 conditions allowed the formation of S-rich secondary sulfides, and only limited desulfurization took place (e.g., replacement of pentlandite by heazlewoodite). Chlorite probably formed at the same conditions as secondary BMMs, as in hydrothermal systems Mg-chlorite forms between 200 and 300 °C (Beaufort et al. 2015), and at different sulfur and oxygen fugacities.

Heazlewoodite, millerite, and Ni–Fe alloys are the most common secondary base metal minerals within ophiolite chromitites (Klein and Bach 2009). The alteration of pentlandite into heazlewoodite occurs below 550 °C, while the formation of Ni–Fe alloys has been estimated at 360–445 °C under reducing conditions (Tzamos et al. 2016). Godlevskite is another common secondary BMM within serpentinized massifs, thought to replace primary sulfides or heazlewoodite during serpentinization (Klein and Bach 2009). Moreover, heazlewoodite and godlevskite can be replaced by millerite if fO_2 and fS_2 increase, like during steatitization of ultramafic rocks (Klein and Bach 2009).

The rich BMM assemblage detected at St. George allows us to constrain the upper temperature of formation of the secondary sulfides, antimonides, and arsenides (Fig. 11C).

Experimental studies (Hewitt 1948) prove that nickeline (NiAs) and breithauptite (NiSb) form solid solutions in artificial melts. However, natural observations reveal that they also can occur together. The coexistence of NiSb and NiAs, also detected at St. George, is explained by Hewitt (1948) as the result of either the replacement of breithauptite by nickeline or with crystallization at low temperatures, in the presence of aqueous fluids, which would prevent the formation of solid solutions. According to Ni-As and Ni-Sb phase diagrams (Yund 1961; Raghavan 2004; Okamoto 2009), maucherite, nickeline, orcelite, breithauptite, and other antimonides are stable over a wide range of temperatures, up to 1000 °C. However, the assemblages maucherite + orcelite and maucherite + nickeline are stable at temperatures below 800 °C, and the antimonide assemblage reported by Bussolesi et al. (2020) suggests crystallization temperatures below 600 °C for St. George secondary BMM suite, or even lower considering the presence of other accessory minerals

such as shandite, whose upper thermal stability is 500 °C (Zhmodik and Agafonov 2000).

The source of metals in the Ni-As-Cu-Sb system is currently unknown. However, the presence of abundant minerals containing As, Cu, Sb, Pb, and Bi, as well as native silver (Economou 1984), supports the hypothesis that Sb, Pb, Bi, Cu, Au, and Ag were metasomatically added during cooling. The occurrence of a metasomatic event in the Gomati ultramafic complex was reported by Scarpelis and Economou (1978), confirming the activity of a fluid phase that can be considered responsible for the crystallization of the rare and accessory phases described in this contribution. Sb-rich porphyry mineralization occurring in the area (Tzamos et al. 2019, 2020) is probably the source of metals, which could have been transported through migrating fluids within fault zones. The Kassandra mining district, located 10 km North of Gomati, hosts porphyry Au-Cu mineralization and Au–Ag–Pb–Zn-Cu carbonate replacement deposits associated with Oligocene–Miocene intrusions emplaced in the metamorphic basement of the Serbo-Macedonian massif. The genesis of these deposits is related to the onset of an extensional regime in the middle Eocene, responsible for the development of widespread normal and transtensional faults (Siron et al. 2018). The fault system in the area is the probable conduit for metasomatic fluids affecting Gomati and generating the low-T mineralogical assemblage.

Evidences from PGE contents

The primary nature of PGE-bearing phases within Tripes, St. George, Limonadika, and Nea Roda chromitites suggests that PGEs were not remobilized during post-magmatic processes. Remobilization of PGEs during secondary processes is often indicated by the presence of PGE alloys and by an Os peak instead of a Ru one in the mantle-normalized PGE patterns (Grieco et al. 2020), which is not present in chromitites from the Gomati and Nea Roda ophiolites (Fig. 12A). The absence of a Ru peak could be also due to the precipitation of Os-Ir rich alloys at high T and low fS_2, but no Os-Ir alloy was detected in Gomati and Nea Roda. Primary PGMs are found mostly enclosed within unaltered chromite and rarely within ferrian chromite rims or in contact with secondary silicates. The euhedral shape of PGMs and their lack of corroded rims suggest that alteration fluids did not affect these minerals. From the base metal sulfide assemblage, we can infer that only limited alteration took place under relatively high fS_2 conditions, as testified by replacement of primary sulfides by secondary ones and not by base metal alloys. Tripes enrichment in PGEs can therefore be explained only by primary processes.

Conclusion

The overall set of mineralogical, textural, and geochemical data helped us to partially constrain the origin of Tripes, St. George, Limonadika, and Nea Roda chromitites. Gomati and Nea Roda ultramafic complexes formed in a suprasubduction geodynamic setting, and the chromitite bodies were generated at different levels of the ophiolite sequence:

- Tripes intermediate chromitites were generated above or at the MTZ, probably within a small magma chamber that crystallized PGE-rich chromitites.
- St. George high-Cr chromitites display features in common with both chromitites generated from boninitic magmas in the mantle but also to some chromitite bodies generated closely above the upper mantle within the Moho transition zone.
- Limonadika high-Cr chromitites show chromite mineral chemistry, PGE contents, and PGE-normalized patterns comparable to typical high-Cr mantle chromitites, and they were likely generated from boninitic magmas in a supra-subduction setting.
- Nea Roda intermediate- to high-Cr chromitites show the lowest PGE contents, suggesting a crystallization from a magma already depleted in PGEs. This could be in agreement with a genesis from an arc-type melt that precipitated high-Cr chromites leaving behind a low-Cr# and PGE-poor residual melt that crystallized Nea Roda PGE-poor intermediate chromitites.

The post-magmatic evolution of Gomati and Nea Roda was dominated by an alteration event related to the circulation of high fO_2 and fS_2 fluids, responsible for the alteration of chromite into ferrian chromite and the replacement of primary silicates by chlorite. The BMMs assemblage was affected by the alteration event. Primary sulfides were replaced by secondary ones, but the high fS_2 conditions prevented the formation of secondary BM alloys. Moreover, the introduction of Cu, Sb, Bi, and As in the system, transported from the Kassandra porphyry deposits through faults, led to the crystallization of low-T antimonides and arsenides. The circulating fluids, however, did not alter the PGMs assemblage, and PGEs were not remobilized, as confirmed also by the Ru peak in the PGE mantle-normalized patterns. The high PGE content at Tripes can be explained by formation of chromitite by an IPGE-enriched melt derived from critical melting of mantle peridotites and by the immobility of PGE during later alteration events occurring at high fS_2.

Supplementary Information The online version contains supplementary material available at https://doi.org/10.1007/s00126-022-01109-z.

Declarations

Conflict of interest The authors declare no competing interests.

References

Ahmed A, Arai S (2002) Unexpectedly high-PGE chromitite from the deeper mantle section of the northern Oman ophiolite and its tectonic implications. Contrib Miner Petrol 143:263–278. https://doi.org/10.1007/s00410-002-0347-8

Anders B, Reischmann T, Kostopoulos D, Poller U (2006) The oldest rocks of Greece: first evidence for a Precambrian terrane within the Pelagonian zone. Geol Mag 143:41–58. https://doi.org/10.1017/S0016756805001111

Andrews DRA, Brenan JM (2002) Phase-equilibrium constraints on the magmatic origin of laurite + Ru-Os-Ir alloy. Can Miner 40:1705–1716. https://doi.org/10.2113/gscanmin.40.6.1705

Arai S, Miura M (2015) Podiform chromitites do form beneath mid-ocean ridges. Lithos 232:143–149. https://doi.org/10.1016/j.lithos.2015.06.015

Arai S, Uesugi J, Ahmed AH (2004) Upper crustal podiform chromitite from the northern Oman ophiolite as the stratigraphically shallowest chromitite in ophiolite and its implication for Cr concentration. Contrib Miner Petrol 147:145–154. https://doi.org/10.1007/s00410-004-0552-8

Ballhaus C, Bockrath C, Wohlgemuth-Ueberwasser C et al (2006) Fractionation of the noble metals by physical processes. Contrib Miner Petrol 152:667–684. https://doi.org/10.1007/s00410-006-0126-z

Beaufort D, Rigault C, Billon S et al (2015) Chlorite and chloritization processes through mixed-layer mineral series in low-temperature geological systems – a review. Clay Miner 50:497–523. https://doi.org/10.1180/claymin.2015.050.4.06

Bockrath C, Ballhaus C, Holzheid A (2004) Stabilities of laurite RuS2 and monosulfide liquid solution at magmatic temperature. Chem Geol 208(1–4):265–271. https://doi.org/10.1016/j.chemgeo.2004.04.016

Bonev N, Dilek Y (2010) Geochemistry and tectonic significance of proto-ophiolitic metamafic units from the Serbo-Macedonian and western Rhodope massifs (Bulgaria-Greece). Int Geol Rev 52:298–335. https://doi.org/10.1080/00206810902757214

Bonev N, Dilek Y, Hanchar JM et al (2012) Nd – Sr – Pb isotopic composition and mantle sources of Triassic rift units in the Serbo-Macedonian and the western Rhodope massifs (Bulgaria – Greece). Geol Mag 149:146–152. https://doi.org/10.1017/S0016756811000938

Bonev N, Ovtcharova-Schaltegger M, Moritz R et al (2013) Peri-Gondwanan Ordovician crustal fragments in the high-grade basement of the eastern Rhodope massif, Bulgaria: evidence from U-Pb LA-ICP-MS zircon geochronology and geochemistry. Geodin Acta 26:207–229. https://doi.org/10.1080/09853111.2013.858942

Bonev N, Moritz R, Borisova M, Filipov P (2018) Therma–volvi–gomati complex of the serbo-macedonian massif, Northern Greece: a middle triassic continental margin ophiolite of Neotethyan origin. J Geol Soc London 176:931–944. https://doi.org/10.1144/jgs2017-130

Brenan JM, Andrews D (2001) High temperature stability of laurite and Ru Os Ir alloy and their role in PGE fractionation in mafic magmas. Can Mineral 39:341–350. https://doi.org/10.2113/gscanmin.39.2.341

Bussolesi M, Zaccarini F, Grieco G, Tzamos E (2020) Rare and new compounds in the Ni-Cu-Sb-As system: first occurrence in the Gomati ophiolite, Greece. Period Miner 89:63–76. https://doi.org/10.2451/2020PM855

Bussolesi M, Grieco G, Cavallo A, Zaccarini F (2022) Different tectonic evolution of fast cooling ophiolite mantles recorded by olivine-spinel geothermometry: case studies from Iballe (Albania) and Nea Roda (Greece). Minerals 12:64. https://doi.org/10.3390/min12010064

Cabri LJ, Laflamme JHG (1981) Analyses of minerals containing platinum-group elements. Platinum-gr Elem Mineral Geol Recover 23:151–173

Centrella S, Putnis A, Lanari P, Austrheim H (2018) Textural and chemical evolution of pyroxene during hydration and deformation: a consequence of retrograde metamorphism. Lithos 296–299:245–264. https://doi.org/10.1016/j.lithos.2017.11.002

Chen C, Su B-X, Xiao Y et al (2019) Intermediate chromitite in Kızıldağ ophiolite (SE Turkey) formed during subduction initiation in Neo-Tethys. Ore Geol Rev 104:88–100. https://doi.org/10.1016/j.oregeorev.2018.10.004

Christodoulou C (1980) The geochemistry of podiform chromite deposits from two ophiolite complexes, Chalkidiki peninsula. Diss Durham Univ, Northern Greece

Colás V, González-Jiménez JM, Camprubí A et al (2019) A reappraisal of the metamorphic history of the Tehuitzingo chromitite, Puebla state, Mexico. Int Geol Rev 61:1706–1727. https://doi.org/10.1080/00206814.2018.1542633

Colás V, Padrón-Navarta JA, González-Jiménez JM et al (2017) The role of silica in the hydrous metamorphism of chromite. Ore Geol Rev 90:274–286. https://doi.org/10.1016/j.oregeorev.2017.02.025

Cornelius NK (2008) UHP metamorphic rocks of the eastern Rhodope massif, NE Greece: new constraints from petrology, geochemistry and zircon ages. In: PhD Thesis, University of Mainz, Germany

Dixon JE, Dimitriadis S (1984) Metamorphosed ophiolitic rocks from the Serbo-Macedonian massif, near Lake Volvi, north-east Greece. Geol Soc Lond Spec Publ 17:603–618

Economou M (1984) On the chemical composition of the chromite ores from the Chalkidiki peninsula, Greece. Ofioliti 123–134

Economou M, Dimou E, Economou G, et al (1986) Chromite deposits of Greece. Chromites UNESCÓS IGCP-197 Proj Metallog ophiolites 129–159

Economou-Eliopoulos M (1996) Platinum-group element distribution in chromite ores from ophiolite complexes : implications for their exploration. Ore Geol Rev 11:363–381. https://doi.org/10.1016/S0169-1368(96)00008-X

Garuti G, Naldrett AJ, Ferrario A (1990) Platinum-group elements in magmatic sulfides from the Ivrea Zone; their control by sulfide assimilation and silicate fractionation. Econ Geol 85:328–336. https://doi.org/10.2113/gsecongeo.85.2.328

Garuti G, Pushkarev EV, Thalhammer OAR, Zaccarini F (2012) Chromitites of the urals (part 1): overview of chromite mineral chemistry and geo-tectonic setting. Ofioliti 37:27–53

Gervilla F, Proenza JA, Frei R et al (2005) Distribution of platinum-group elements and Os isotopes in chromite ores from Mayarí-Baracoa ophiolitic belt (eastern Cuba). Contrib Miner Petrol 150:589–607. https://doi.org/10.1007/s00410-005-0039-2

Gervilla F, Padrón-Navarta JA, Kerestedjian T et al (2012) Formation of ferrian chromite in podiform chromitites from the Golyamo Kamenyane serpentinite, eastern Rhodopes, SE Bulgaria: a two-stage process. Contrib Miner Petrol 164:643–657. https://doi.org/10.1007/s00410-012-0763-3

González-Jiménez JM, Kerestedjian T, Proenza JA, Gervilla F (2009) Metamorphism on chromite ores from the Dobromirtsi ultramafic massif, Rhodope mountains (SE Bulgaria). Geol Acta 7:413–429. https://doi.org/10.1344/104.000001447

González-Jiménez JM, Proenza JA, Gervilla F et al (2011) High-Cr and high-Al chromitites from the Sagua de Tánamo district, Mayarí-Cristal ophiolitic massif (eastern Cuba): constraints on their origin from mineralogy and geochemistry of chromian spinel and platinum-group elements. Lithos 125:101–121. https://doi.org/10.1016/j.lithos.2011.01.016

González-Jiménez JM, Griffin WL, Gervilla F et al (2014a) Chromitites in ophiolites: how, where, when, why? Part I. A review and new ideas on the origin and significance of platinum-group minerals. Lithos 189:127–139. https://doi.org/10.1016/j.lithos.2013.06.016

González-Jiménez JM, Griffin WL, Proenza JA et al (2014b) Chromitites in ophiolites: how, where, when, why? Part II The crystallization of chromitites. Lithos 189:140–158. https://doi.org/10.1016/j.lithos.2013.09.008

Good DJ, Crocket JH, Barnett RL (1997) A secondary clinopyroxene-chlorite-spinel assemblage in clinopyroxenite of the Mann complex, Abitibi Belt, Ontario: an unusual hydrothermal alteration suite. Miner Petrol 59:69–90. https://doi.org/10.1007/BF01163062

Grieco G, Diella V, Chaplygina NL, Savelieva GN (2007) Platinum group elements zoning and mineralogy of chromitites from the cumulate sequence of the Nurali massif (southern Urals, Russia). Ore Geol Rev 30:257–276. https://doi.org/10.1016/j.oregeorev.2006.03.002

Grieco G, Bussolesi M, Eslami A et al (2020) Differential platinum group elements (PGE) re-mobilization at low fS2 in Abdasht and Soghan mafic-ultramafic complexes (southern Iran). Lithos 366–367:105523. https://doi.org/10.1016/j.lithos.2020.105523

Helgadóttir HM, Franzson H, Óskarsson N, et al (2015) Hydrothermal alteration of pyroxene in the Hellisheiði geothermal field, SW-Iceland. In: Proceedings World Geothermal Congress

Hewitt DF (1948) A partial study of the NiAs-NiSb system. Econ Geol 43:408–417

Hey MH (1954) A new review of the chlorites. Miner Mag J Miner Soc 30:277–292

Himmerikus F, Reischmann T, Kostopoulos D (2009) Triassic rift-related meta-granites in the Internal Hellenides, Greece. Geol Mag 146:252–265. https://doi.org/10.1017/S001675680800592X

Kapsiotis AN (2015) Alteration of chromitites from the Voidolakkos and Xerolivado mines, Vourinos ophiolite complex, Greece: implications for deformation-induced metamorphism. Geol J 50:739–763. https://doi.org/10.1002/gj.2590

Kimball KL (1990) Effects of hydrothermal alteration on the compositions of chromian spinels. Contrib Miner Petrol 105:337–346. https://doi.org/10.1007/BF00306543

Klein F, Bach W (2009) Fe-Ni-Co-O-S phase relations in peridotite-seawater interactions. J Petrol 50:37–59. https://doi.org/10.1093/petrology/egn071

Kockel F (1977) Erläuterungen zur Geologischen Karte der Chalkidhiki und angrenzender Gebiete 1: 100 000 (Nord-Griechenland). Bundesanstalt für Geowissenschaften und Rohstoffe

Kockel F, Mollat H, Walther HW (1971) Geologie des Serbo-macedonischen massivs und seines mesozoichen rahmens (Nordgriecheland). Geol Jahrb 89:529–551

Kockel F, Mollat H, Antoniadis P (1978) Geological map of Greece, Ierissos sheet. Inst Geol Miner Explor Greece Scale 1(50):000

Kullerud G (1969) Phase relations in the Cu-Fe-S, Cu-Ni-S and Fe-Ni-S system. Magmat ORE Depos 323–343

Langa MM, Jugo PJ, Leybourne MI et al (2021) Chromite chemistry of a massive chromitite seam in the northern limb of the Bushveld igneous complex, South Africa: correlation with the UG-2 in the eastern and western limbs and evidence of variable assimilation of footwall rocks. Miner Depos 56:31–44. https://doi.org/10.1007/s00126-020-00964-y

Legendre O, Augé T (1986) Mineralogy of platinum-group mineral inclusions in chromtites from different ophiolitic complexes. In: Conference metallogeny of basic and ultrabasic rocks, pp 361–372

Liu X, Su B-X, Xiao Y et al (2019) Initial subduction of Neo-Tethyan ocean: geochemical records in chromite and mineral inclusions in the Pozantı-Karsantı ophiolite, southern Turkey. Ore Geol Rev 110:102926. https://doi.org/10.1016/j.oregeorev.2019.05.012

Lorand J-P, Alard O (2001) Platinum-group element abundances in the upper mantle: new constraints from in situ and whole-rock analyses of massif central xenoliths (France). Geochim Cosmochim Acta 65:2789–2806. https://doi.org/10.1016/S0016-7037(01)00627-5

Malitch KN, Thalhammer OA, Knauf VV, Melcher F (2003) Diversity of platinum-group mineral assemblages in banded and podiform chromitite from the Kraubath ultramafic massif, Austria: evidence for an ophiolitic transition zone? Miner Depos 38:282–297. https://doi.org/10.1007/s00126-002-0308-1

McDonough WF, Sun SS (1995) The composition of the earth. Chem Geol 120:223–253. https://doi.org/10.1016/0009-2541(94)00140-4

Merlini A, Grieco G, Diella V (2009) Ferritchromite and chromian-chlorite formation in mélange-hosted Kalkan chromitite (southern Urals, Russia). Am Miner 94:1459–1467. https://doi.org/10.2138/am.2009.3082

Michailidis KM, Soldatos TC, Christodoulou C (1995) Ultramafic rocks and associated chromite mineralisation from Nea Roda (eastern Chalkidiki peninsula, Northern Greece). Ofioliti 20:81–96

Naldrett T, Kinnaird J, Wilson A, Chunnett G (2008) Concentration of PGE in the earth's crust with special reference to the Bushveld complex. Earth Sci Front 15:264–297. https://doi.org/10.1016/S1872-5791(09)60006-3

Okamoto H (2009) Ni-Sb (nickel-antimony). J Phase Equilibria Diffus 30:301–302

Pagé P, Barnes S-J (2009) Using trace elements in chromites to constrain the origin of podiform chromitites in the Thetford Mines ophiolite, Québec, Canada. Econ Geol 104:997–1018

Papanikolaou D (2013) Tectonostratigraphic models of the Alpine terranes and subduction history of the Hellenides. Tectonophysics 595–596:1–24. https://doi.org/10.1016/j.tecto.2012.08.008

Prichard HM, Neary CR, Fisher PC, O'Hara MJ (2008) PGE-rich podiform chromitites in the Al 'Ays ophiolite complex, Saudi Arabia: an example of critical mantle melting to extract and concentrate PGE. Econ Geol 103:1507–1529. https://doi.org/10.2113/gseco ngeo.103.7.1507

Prichard HM, Tarkian M (1988) Platinum and palladium minerals from two PGE-rich localities in the Shetland ophiolite complex. Can Miner 26:979–990

Proenza J, Solé J, Melgarejo JC (1999a) Uvarovite in podiform chromitite; the Moa-Baracoa ophiolitic massif. Cuba Can Miner 37:679–690

Proenza JA, Melgarejo JC, Bodinier JL (1999b) Al- and Cr-rich chromitites from the Mayarì-Baracoa ophiolitic belt (eastern Cuba): consequence of interaction between volatile-rich melts and peridotites in suprasubduction mantle. Econ Geol 94:547–566

Qiu T, Yang J, Milushi I et al (2018) Petrology and PGE abundances of high-Cr and high-Al podiform chromitites and peridotites from the Bulqiza ultramafic massif, eastern Mirdita ophiolite, Albania. Acta Geol Sin - English Ed 92:1063–1081. https://doi.org/10.1111/1755-6724.13592

Raghavan V (2004) Fe-Ni-Sb (iron-nickel-antimony). J Phase Equilibria Diffus 25:553

Ricou L, Burg J, Godfriaux I et al (1998) Rhodope and Vardar : the metamorphic and the olistostromic paired belts related to the cretaceous subduction under Europe Rhodope and Vardar : the metamorphic and the olistostromic paired belts related to the cretaceous subduction under Europe. Geodin Acta 11:285–309

Rollinson H (2008) The geochemistry of mantle chromitites from the northern part of the Oman ophiolite: inferred parental melt compositions. Contrib Miner Petrol 156:273–288. https://doi.org/10.1007/s00410-008-0284-2

Scarpelis N, Economou M (1978) Genesis and metasomatism of chromite ore from the Gomati area, Chalkidiki, Greece. Ann Geol Pays Hell 29:716–728

Siron CR, Rhys D, Thompson JFH et al (2018) Structural controls on porphyry Au-Cu and Au-rich polymetallic carbonate-hosted replacement deposits of the Kassandra mining district, Northern Greece. Econ Geol 113:309–345. https://doi.org/10.5382/econgeo.2018.4552

Šoster A, Zavašnik J, O'Sullivan P et al (2020) Geochemistry of Bashibos-Bajrambos metasedimentary unit, Serbo-Macedonian massif, North Macedonia: implications for age, provenance and tectonic setting. Geochemistry 80:125664. https://doi.org/10.1016/j.chemer.2020.125664

Stowe CW (1994) Compositions and tectonic settings of chromite deposits through time. Econ Geol 89:528–546

Torres-Ruiz J, Garuti G, Gazzotti M et al (1996) Platinum-group minerals in chromitites from the ojen lherzolite massif (Serrania de Ronda, Betic Cordillera, Southern Spain). Mineral Petrol 56:25–50. https://doi.org/10.1007/BF01162656J

Tzamos E, Filippidis A, Michailidis K et al (2016) Mineral chemistry and formation of awaruite and heazlewoodite in the Xerolivado chrome mine, Vourinos, Greece. Bull Geol Soc Greece 50:2047–2056

Tzamos E, Papadopoulos A, Grieco G et al (2019) Investigation of trace and critical elements (including actinides) in flotation sulphide concentrates of Kassandra mines (Chalkidiki, Greece). Geosciences 9:164. https://doi.org/10.3390/geosciences9040164

Tzamos E, Gamaletsos PN, Grieco G et al (2020) New insights into the mineralogy and geochemistry of Sb ores from Greece. Minerals 10:236. https://doi.org/10.3390/min10030236

Uysal I, Akmaz RM, Saka S, Kapsiotis A (2016) Coexistence of compositionally heterogeneous chromitites in the Antalya-Isparta ophiolitic suite, SW Turkey: a record of sequential magmatic processes in the sub-arc lithospheric mantle. Lithos 248–251:160–174. https://doi.org/10.1016/j.lithos.2016.01.021

Uysal I, Kapsiotis A, Akmaz RM et al (2018) The Guleman ophiolitic chromitites (SE Turkey) and their link to a compositionally evolving mantle source during subduction initiation. Ore Geol Rev 93:98–113. https://doi.org/10.1016/j.oregeorev.2017.12.017

Uysal İ, Tarkian M, Sadiklar MB et al (2009) Petrology of Al- and Cr-rich ophiolitic chromitites from the Muğla, SW Turkey: implications from composition of chromite, solid inclusions of platinum-group mineral, silicate, and base-metal mineral, and Os-isotope geochemistry. Contrib Miner Petrol 158:659–674. https://doi.org/10.1007/s00410-009-0402-9

Xiong F, Yang J, Robinson PT et al (2017) High-Al and high-Cr podiform chromitites from the western Yarlung-Zangbo suture zone, Tibet: implications from mineralogy and geochemistry of chromian spinel, and platinum-group elements. Ore Geol Rev 80:1020–1041. https://doi.org/10.1016/j.oregeorev.2016.09.009

Yund RA (1961) Phase relations in the system Ni-As. Econ Geol 56:1273–1296. https://doi.org/10.2113/gsecongeo.56.7.1273

Zaccarini F, Pushkarev EV, Fershtater GB, Garuti G (2004) Composition and mineralogy of PGE-rich chromitites in the Nurali lherzolite gabbro complex, southern Urals, Russia. Can Miner 42:545–562. https://doi.org/10.2113/gscanmin.42.2.545

Zaccarini F, Singh AK, Garuti G (2016) Platinum group minerals and silicate inclusions in chromitite from the Naga-Manipur ophiolite complex, Indo-Myanmar orogenic belt, northeast India. Can Miner 54:409–427. https://doi.org/10.3749/canmin.1500034

Zachariadis PT (2007) Ophiolites of the eastern Vardar zone, N. Greece. In: PhD Thesis, University of Mainz, Germany

Zhmodik SM, Agafonov LV (2000) Shandite and other nickel minerals from chromitites of ophiolite association in the southeast of East Sayan. Geol i Geofiz 41:712–721

Zhou M-F, Robinson PT (1997) Origin and tectonic environment of podiform chromite deposits. Econ Geol 92:259–262. https://doi.org/10.2113/gsecongeo.92.2.259

Zhou M-F, Robinson PT, Malpas J et al (2001) Melt/mantle interaction and melt evolution in the Sartohay high-Al chromite deposits of the Dalabute ophiolite (NW China). J Asian Earth Sci 19:517–534. https://doi.org/10.1016/S1367-9120(00)00048-1

Zhou M-F, Robinson PT, Su B-X et al (2014) Compositions of chromite, associated minerals, and parental magmas of podiform chromite deposits: the role of slab contamination of asthenospheric melts in suprasubduction zone environments. Gondwana Res 26:262–283. https://doi.org/10.1016/j.gr.2013.12.011

Zhou M-F, Sun M, Keays RR, Kerrich RW (1998) Controls on platinum-group elemental distributions of podiform chromitites: a case study of high-Cr and high-Al chromitites from Chinese orogenic belts. Geochim Cosmochim Acta 62:677–688. https://doi.org/10.1016/S0016-7037(97)00382-7